

Copy 1

GUGGENHEIM AERONAUTICAL LABORATORY
CALIFORNIA INSTITUTE OF TECHNOLOGY

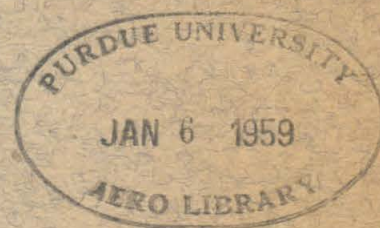
HYPersonic RESEARCH PROJECT

Memorandum No. 46

September 25, 1958

**INVESTIGATION OF THE TRANSMISSION
OF A SHOCK WAVE THROUGH AN ORIFICE**

by
Louis L. Monroe



ARMY ORDNANCE CONTRACT NO. DA-04-495-Ord-19

GUGGENHEIM AERONAUTICAL LABORATORY
CALIFORNIA INSTITUTE OF TECHNOLOGY
Pasadena, California

HYPERSONIC RESEARCH PROJECT

Memorandum No. 46

September 25, 1958

INVESTIGATION OF THE TRANSMISSION
OF A SHOCK WAVE THROUGH AN ORIFICE

by

Louis L. Monroe


Clark B. Millikan, Director
Guggenheim Aeronautical Laboratory

ARMY ORDNANCE CONTRACT NO. DA-04-495-Ord-19
Army Project No. 5B0306004
Ordnance Project No. TB3-0118
OOR Project No. 1600-PE

ACKNOWLEDGMENTS

The author expresses his deep appreciation to Professor Anatol Roshko and Professor Lester Lees for their suggestions, guidance and encouragement throughout the course of this investigation and for their kind assistance in the preparation of this manuscript.

Thanks are also extended to Mrs. Gerry Van Gieson for typing of the manuscript, to Mrs. Betty Laue for preparing the figures, and to Mrs. Truus van Harreveld for her able handling of the numerical calculations.

ABSTRACT

A shock wave propagating in air in a shock tube was reflected from an orifice plate, and the strength or Mach number of the transmitted wave was measured for a range of incident shock Mach numbers from 3 to 9 for several types of orifices. Also schlieren photographs of the starting flow pattern were made for some of the orifices investigated.

The measured values of transmitted shock strength are compared with predicted values based on a theoretical one-dimensional flow model for both an ideal gas and a real gas. The agreement between the measured values of transmitted wave Mach number and the theoretically predicted values is extremely good in the Mach number range investigated for a wedge type orifice at an ambient shock tube pressure of 5.0 mm Hg, and also for a conical type orifice at an ambient shock tube pressure of 2.5 mm Hg. For both orifices the ratio of outlet area to inlet area is 7.67.

The data also indicate that for a wedge type orifice of area ratio of 23.0 and for a plate (free expansion) type orifice of area ratio 23.0 possible boundary layer and shock wave interactions downstream of the orifice result in measured values of transmitted wave Mach number somewhat greater than that predicted by the one-dimensional flow model.

Investigation of the conical orifice with an area ratio 7.67 at a low ambient pressure in the shock tube (0.4 mm Hg) also yields measured values of transmitted wave Mach number greater than that predicted by the one-dimensional flow model, indicating the probable development of a thick boundary layer behind the transmitted wave downstream of the orifice.

TABLE OF CONTENTS

PART		PAGE
	Acknowledgments	ii
	Abstract	iii
	Table of Contents	iv
	List of Figures	vi
	Nomenclature and List of Symbols	viii
I.	Introduction	1
II.	Description of Research Facility, Model Installation and Instrumentation	3
III.	Discussion of the Theoretical One-Dimensional Flow Model	6
	A. Ideal Gas - Predicted Transmitted Wave Speeds	8
	B. Equilibrium Air - Predicted Transmitted Wave Speeds	9
IV.	Orifice and Nozzle Configurations	13
V.	Discussion of Results	15
	A. Schlieren Studies	15
	B. Measured Values of Transmitted Wave Speeds	16
	1. Introductory Remarks	16
	2. Configuration A, Wedge Type Orifice, Area Ratio $A_6/A_* = 7.67$	17
	3. Configuration B, Plate-Type Orifice Area Ratio $A_6/A_* = 7.67$	18
	4. Configuration C, Wedge-Type Orifice Configuration D, Plate-Type Orifice, Sharp Edge Configuration D, Plate-Type Orifice, Round Edge (Area Ratio A_6/A_* for All 3 Orifices = 23)	18

5.	Configuration F, Conical Type Orifice Area Ratio $A_6/A_* = 7.67$	19
a.	Ambient Pressure, $P_1 = 2.5$ mm Hg	19
b.	Ambient Pressure, $P_1 = 0.4$ mm Hg	20
VI.	Concluding Remarks	22
	References	23
Appendix I	-- Outline of Procedure for Calculating the Predicted Values of the Transmitted Wave Speeds, M_{sq} , for an Ideal Gas Based on the Theoretical One-Dimensional Model Described in This Report	24
Appendix II	-- Outline of Procedure for Calculating the Predicted Values of the Transmitted Wave Speeds, M_{sq} , in Equilibrium Air Based on the Theoretical One- Dimensional Model Described in This Report	30 30
	Figures	34

LIST OF FIGURES

NUMBER		PAGE
1	Typical Model Installation in 2-7/8" x 2-7/8" Shock Tube Showing Location of Model and Heat Gages	34
2	Typical Oscilloscope Records for Measuring the Transmitted Wave Speed	35
3	Schematic of Flow Regions	36
4	Calculated Values of Velocity Ratios and Mach Numbers Based on Theoretical One Dimensional Model for Ideal Gas ($\gamma = 1.40$), Area Ratio $A_6/A_* = 7.67$	37
5	Calculated Values of Velocity Ratios and Mach Numbers Based on Theoretical One Dimensional Model for Ideal Gas ($\gamma = 1.40$), Area Ratio $A_6/A_* = 23.0$	38
6	Temperatures in Region 5 Behind the Reflected Shock Wave for Ideal Gas and Real Gas. Ambient Shock Tube Temperature $T_1 = 300^\circ\text{K}$	39
7	Calculated Values of Velocity Ratios and Mach Numbers Based on Theoretical One Dimensional Flow Model for Equilibrium Air and for Ideal Gas ($\gamma = 1.40$), Area Ratio $A_6/A_* = 7.67$	40
8	Calculated Values of Enthalpy in Flow Regions 5, 6, and 7 Based on Theoretical One Dimensional Flow Model for Equilibrium Air and for Ideal Gas ($\gamma = 1.40$), Area Ratio $A_6/A_* = 7.67$	41
9	Calculated Values of Pressure Ratios in Flow Regions 5, 6, and 7 Based on Theoretical One Dimensional Flow Model for Equilibrium Air and for Ideal Gas ($\gamma = 1.40$), Area Ratio $A_6/A_* = 7.67$	42
10	Photographs and Sketches of Profile of Flow Passage through Orifices as Seen through Viewing Opening in Shock Tube	43-46

11	Configuration E, Channel Type Orifice, Sequence of Schlieren Photographs Showing the Incident Wave Reflecting from the Face of the Model, and Also the Subsequent Waves. $M_{su} = 5.0$ (Approximately)	47
12	Configuration B, Plate Type Orifice, Sequence of Schlieren Photographs Showing the Waves of the Starting Flow Process and the Transmitted Wave, M_{sd}	48-49
13	Comparison of Measured Values and Theoretical One Dimensional Model Predicted Values of Mach Number of Transmitted Wave. Configuration A, Wedge-Type Orifice, Area Ratio $A_6/A_* = 7.67$	50
14	Comparison of Measured Values and Theoretical One Dimensional Model Predicted Values of Mach Number of Transmitted Wave. Configuration B, Plate-Type Orifice, Area Ratio $A_6/A_* = 7.67$	51
15	Comparison of Transmitted Wave Mach Numbers of Configurations A and B	52
16	Comparison of Measured Values and Theoretical One Dimensional Model Predicted Values of Transmitted Wave Mach Numbers. Configurations C and D, Area Ratio $A_6/A_* = 23$	53
17	Comparison of Measured Values and Theoretical One Dimensional Model Predicted Values of Transmitted Wave Mach Numbers. Configuration F, Conical Type Orifice, Area Ratio $A_6/A_* = 7.67$	54

NOMENCLATURE AND LIST OF SYMBOLS

M	Mach number
W	wave speed in + x- direction relative to stationary laboratory coordinates
$(W)_r$	wave speed in + x- direction relative to the fluid into which the wave is advancing
W_c	wave speed of the starting compression shock wave relative to stationary laboratory coordinates
$(W_c)_r$	wave speed of the starting compression shock wave relative to the fluid into which the wave is advancing
M_{su}	$= \frac{W_{su}}{a_1} =$ Mach number of incident (upstream) shock wave
M_{s2}	$= \frac{W_2}{a_2} =$ Mach number of wave reflected from orifice plate
M_{sd}	$= \frac{W_{sd}}{a_9} =$ Mach number of transmitted (downstream) shock wave
$(M_c)_r$	$= \frac{(W_c)_r}{a_6} =$ Mach number of the starting compression shock wave, relative to the fluid into which it is advancing
P	static pressure
T	temperature
ρ	density
h	enthalpy
S	entropy
U	flow velocity
A	area
a	sonic velocity
γ	ratio of specific heats
R	gas constant

Subscripts

All numerical subscripts refer to the flow region along the tube indicated in Figure 4. For example, U_6 refers to the flow velocity in region 6.

The subscript * refers to conditions at the inlet or throat of the orifice opening.

I. INTRODUCTION

When an incident shock wave strikes a solid wall, a reflected wave is generated. Behind this reflected wave there is a region of high stagnation pressure and enthalpy. If a hole or orifice is drilled in the solid wall to form a nozzle, this stagnation region can be utilized as a reservoir of energy for generating a high Mach number, high enthalpy flow downstream of the nozzle (region 6 of Figure 3) by allowing the flow to expand through the orifice as shown.

Several questions arise in connection with this process. In particular, what does the starting flow through the nozzle orifice look like, and what is the intensity of the shock wave that is transmitted through the orifice opening? This report attempts to answer some of these questions, particularly with regard to the intensity of the wave transmitted through the orifice for any arbitrary strength of incident wave (up to incident shock Mach number of 9.0) for several types of orifices.

A study somewhat related to the present investigation, but in connection with wire screens, is described in Reference 4, in which a plane shock wave interacts with wire screens of fifty per cent and sixty-two per cent blockage, corresponding to ratios of tube area to open screen area of 2.0 and 2.63, respectively. Comparisons of measured and predicted values of transmitted wave Mach number are made for the case of an ideal gas for incident wave Mach numbers up to about 3.25.

This present report discusses the results of a shock tube

investigation of several types of nozzle orifices (wedge, conical and free expansion) of considerably smaller flow openings than those of Reference 4, namely, ratios of tube area to orifice inlet area of 7.67 and 23.0 (Figure 10). Comparison between measured and predicted values of transmitted wave speeds is made for both an ideal gas and equilibrium air for incident shock Mach number between 3.0 and 9.0 (incident shock wave pressure ratios, P_2/P_1 , of 10 to 95). The ambient shock tube pressures in the low pressure chamber range from 14.0 mm Hg down to 0.4 mm Hg.

The configurations investigated herein are described in Section IV. A discussion of the theoretical one-dimensional flow model for calculating the value of the predicted transmitted shock wave Mach number is presented in Section III (and in Appendices I and II) for the case of an ideal gas and also for a real gas (equilibrium air).

Section V contains the discussion of the experimental results, including schlieren photographs of the starting flow, measured transmitted wave speeds for the orifices investigated at several ambient shock tube pressures, and a comparison of the above measured results with those predicted by the one-dimensional flow model.

II. DESCRIPTION OF RESEARCH FACILITY, MODEL INSTALLATION AND INSTRUMENTATION

For incident shock Mach numbers of 3 to 6, the 2-7/8" x 2-7/8" GALCIT shock tube described in Reference 1 was utilized for the study of configurations A to E. The 2-inch round GALCIT shock tube was utilized in the study of configuration F for a range of incident shock Mach numbers of 4 to 9. (A description of the configurations investigated is presented in Section IV.) Both of these shock tubes are of rather conventional design. Driver gases for the tube are either high pressure helium or nitrogen. Driver gas pressures up to 600 pounds per square inch were utilized. Most of the measurements in this report were made with unheated helium as the driver gas.

The driven gas (i. e., the gas in the low pressure chamber) was air at all times. Ambient or initial pressures in the low pressure chamber were maintained by a high vacuum, Welch Duo-Seal vacuum pump which could bring the round shock tube system rapidly down to 0.40 mm Hg. The high and low pressure chambers of the tube were separated by copper diaphragms of either .005" or .010" thickness scribed so as to rupture at approximately the desired pressure. Exact regulation of the bursting pressure of the diaphragm was not required inasmuch as the incident shock speeds were measured each time by an accurate electronic counter-timer as described in Section II.

A sketch of a typical orifice model and instrumentation installation in one of the shock tubes is shown in Figure 1. The incident wave speed was determined by the time required for the wave to travel

between two fixed points in the tube upstream of the orifice, as shown in Figure 1. The elapsed time was measured directly on a model 7360 Berkeley counter, accurate to within one microsecond. The counter was started and stopped through pulse-type amplifiers by means of platinum resistance heat gages mounted flush with the walls of the tube (Reference 1).

The relatively constant speed of the incident (upstream) wave is demonstrated in Reference 1. In this reference the shock wave attenuation is calculated to be less than about 4 per cent in the case of a laminar boundary layer for a 20-foot tube (or less than 0.4 per cent over the 2-foot span between heat gages in the rectangular tube). It is estimated in Reference 1 that the upstream wave speed can be measured to an accuracy of $\frac{1}{2}$ per cent.

The speed of the transmitted wave was indicated on the screen of a Tektronix type 525 high speed oscilloscope as follows: The three heat gages shown in Figure 1 downstream of the orifice were connected in series with the input circuit to the oscilloscope. The arrival of the moving transmitted wave at each of the three heat gages is indicated on the oscilloscope records by a sharp rise (step function) in the input pattern. Typical oscilloscope records are shown in Figure 2; these were made by photographing the oscilloscope screen with a Polaroid Land camera.

For almost all conditions investigated, the transmitted shock wave moved at a steady, uniform velocity in the constant area of the tube, as indicated on the oscilloscope records by equal values of the time required for the wave to travel equal distances at different locations

along the tube. It is estimated that the measuring technique of the transmitted wave speed is accurate to about 2 per cent.

Schlieren photographs were made by means of a high speed spark discharge system utilizing a capacitor-thyratron discharge spark unit of about 2 micro-second spark duration time, as described in Reference 1. The spark was triggered through an adjustable electronic time delay unit by means of one of the resistance heat gages. The time delay unit was calibrated in micro-seconds. The lens-mirror system was such that satisfactory schlieren photographs could be made at densities of the order of 3×10^{-2} atmospheres behind the moving shock wave (Reference 1).

III. DISCUSSION OF THE THEORETICAL ONE-DIMENSIONAL FLOW MODEL

For the purpose of predicting the intensity or Mach number of the transmitted wave for any arbitrary value of incident shock Mach number, it was assumed that the flow process could be represented by a one-dimensional model as shown in Figure 3. The incident shock wave advances into stationary air in region 1, leaving behind it a region of increased pressure, temperature and velocity described as region 2. When the incident wave strikes the walls of the orifice, it generates a reflected wave which further increases the pressure and enthalpy in the region 5 behind it. The resulting large pressure difference between regions 5 and 6 produces a high velocity flow, U_6 , and a strong transmitted shock wave whose Mach number is denoted by M_{sd} . This wave is transmitted downstream from the orifice, advancing into the stationary air of region 9, and leaving behind it a region 8, of increased pressure and enthalpy.

The expansion of the starting flow just downstream of the orifice reduces the static pressure as in any ordinary flow expansion. In order to satisfy the physical condition of a low pressure in region 6 and a high pressure in region 8 a starting compression shock $(W_c)_r$ forms which tends to propagate upstream against the flow. Also, there exists an interface or contact surface separating region 7 from region 8; across this contact surface there is a discontinuous change in entropy, temperature and density but no change in flow velocity or pressure.

For the purpose of the theoretical, one-dimensional model

calculations it is assumed that the starting compression wave $(W_c)_r$ downstream of the orifice is a plane wave. Although this starting compression wave propagates upstream relative to the advancing flow, nevertheless, for the particular area ratios of orifices investigated, the flow velocity in region 6 is at all times greater than the relative starting wave velocity $(W_c)_r$, so that the wave is actually carried downstream by the flow, relative to the stationary shock tube walls. The assumption is made that this wave moves at uniform speed.

It is also assumed that the flow through the orifice expands isentropically into region 6 to the full area of the tube downstream of the orifice. Both the 2-7/8" x 2-7/8" tube and the 2" round tube are constant area shock tubes and so for each model investigated $A_5 = A_6 = A_9$.

On the basis of the foregoing one-dimensional model of the flow, one can calculate the Mach number of the transmitted wave for any arbitrary Mach number, M_{su} , of the incident wave. For convenience in comparing the ideal gas and real gas flow conditions and wave speeds along the tube the same general stepwise calculation procedure was used for both the ideal gas and real gas (equilibrium air) calculations.*

* An analytical procedure for the calculation of predicted wave speeds based on the flow of an ideal gas through a wire screen is discussed in Reference 4 for low values of incident shock Mach number. However, the equations of Reference 4 are not applicable to real gas calculations.

A. Ideal Gas - Predicted Transmitted Wave Speeds

An outline of the procedure used in this report for calculating the predicted values of the transmitted wave speeds for an ideal gas based on the theoretical one-dimensional flow model is presented in Appendix I. The results of the calculations outlined in Appendix I for an ideal gas ($\gamma = 1.40$) are shown in Figures 4 and 5 for the two area ratios investigated. In particular, one should note that the magnitude of the Mach number, $(M_c)_r$ of the starting compression wave is only slightly less than M_6 , the flow Mach number in region 6, indicating that $(M_c)_r$ is a relatively strong shock wave, and that it moves downstream along the tube very slowly relative to the stationary laboratory coordinates.

Also, the calculations indicate that the strength or Mach number of the starting shock wave, $(M_c)_r$ increases as the area ratio A_6/A_* is increased from 7.67 to 23.0. In fact, for only a slightly larger area ratio than investigated, the starting shock wave $(W_c)_r$ would cease to move down the tube and would locate itself, as a stationary wave, in the divergent part of the expanding orifice section.

The fact that the value of $(M_c)_r$ is large at even moderate area ratios A_6/A_* indicates clearly why, as discussed in Reference 2, a diaphragm is needed at the inlet to the orifice for satisfactory operation of a hypersonic shock tube. That is, the starting pressure, P_9 , downstream of the orifice must be considerably less than the initial ambient pressure, P_1 , so that the starting compression wave, $(M_c)_r$ is sufficiently weakened to allow it to be carried swiftly out of the tube by the prevailing flow, U_6 .

Figures 4 and 5 also show that for each area ratio A_6/A_* the value of M_6 is constant for all values of M_{su} , as is to be expected for an ideal gas (M_6 depends only on the area ratio, A_6/A_*). The almost linear increase of U_6/a_1 with increasing M_{su} also follows directly from the ideal gas theory; i. e.,

$$\frac{U_6}{a_1} = \frac{U_6}{a_6} \cdot \frac{a_6}{a_5} \cdot \frac{a_5}{a_2} \cdot \frac{a_2}{a_1}$$

Equation (2) of Appendix I shows that a_2/a_1 is almost directly proportional to M_{su} at the higher values of M_{su} . Similarly, a_5/a_2 varies linearly with M_{s2} . But M_{s2} happens to vary very slowly with M_{su} so that a_5/a_2 varies very slowly. Inasmuch as U_6/a_6 and a_6/a_5 depend only on the area ratio, A_6/A_* , and therefore are constant, the result is that U_6/a_1 varies almost linearly with a_2/a_1 and therefore almost linearly with M_{su} .

In regard to the speed of the transmitted wave, M_{sd} it can also be seen from Figures 4 and 5 that the strength of the starting shock wave $(M_c)_r$ has an important effect on the strength of the transmitted wave; in general, the stronger this shock wave, the weaker is the transmitted wave.

B. Equilibrium Air - Predicted Transmitted Wave Speeds

The equations of Appendix I for an ideal gas are, of course, not applicable for calculations involving real gas effects. The temperatures in degrees Kelvin behind the reflected shock wave in region 5, calculated for both an ideal gas and for equilibrium air, are indicated in Figure 6. It can be seen from this figure that the real gas effects

become significant at a fairly low value of M_{su} . Accordingly, calculations were made of predicted wave speeds for a real gas based on the one-dimensional flow model. These real gas calculations are outlined in Appendix II and were made by a stepwise procedure along the tube somewhat similar in principle to that described in Appendix I for an ideal gas, except that the tables and Mollier diagram for equilibrium air of Reference 3 were utilized for the thermodynamic properties of the real gas. The changes in the flow conditions across the incident shock wave, M_{su} , across the starting compression wave $(W_c)_r$, and across the transmitted wave M_{sd} were calculated by iteration methods, by direct resort to the basic equations of motion of a moving shock wave in a real gas.

The results of the calculations discussed in Appendix II for equilibrium air, for the area ratio $A_6/A_* = 7.67$ (corresponding to the area ratio for configuration F discussed later in this report) are shown in Figures 7, 8, and 9 for a range of incident shock Mach numbers up to $M_{su} = 10$, and were calculated for an ambient shock tube pressure, $P_1 = 1.0$ mm Hg and an ambient tube temperature $T_1 = 300^\circ\text{K}$. These results are compared in Figures 7, 8, and 9 with the corresponding results of the calculations for an ideal gas. It should be noticed that despite the tremendous difference in temperatures in region 5 behind the reflected shock wave of an ideal and real gas (Figure 6), the calculated values of the predicted transmitted wave speeds of the real gas and those of the ideal gas are surprisingly almost identical (Figure 7).

This somewhat unexpected result is shown below to be rather a

coincidence and is the result of several compensating flow effects.

For an ideal gas, $\gamma = \text{constant}$, but for a real gas, as the enthalpy of the gas is increased, the higher degrees of freedom such as rotation and vibration become excited and also dissociation of the gas begins to occur. All of these effects tend to reduce the value of γ for a real gas at the higher temperatures. But for region 6, equation (9) of Appendix I can be written as,

$$\left(\frac{A_6}{A_*} \right)^{\frac{2(\gamma-1)}{\gamma+1}} = \frac{1}{M_6} \left[\frac{1 + \frac{\gamma-1}{2} (M_6)^2}{1 + \frac{\gamma-1}{2}} \right]$$

and from the energy equation,

$$\frac{U_6^2}{2} + h_6 = \frac{U_5^2}{2} + h_5$$

one can show (for $U_5 = 0$) that,

$$\frac{U_6^2}{2h_5} = \frac{\frac{\gamma-1}{2} M_6^2}{1 + \frac{\gamma-1}{2} M_6^2}$$

Therefore, from the above equations, one can see that for a specified area ratio, A_6/A_* , the resulting M_6 and U_6 are reduced as γ is reduced. Also, as the value of γ is reduced a larger area ratio A_6/A_* is needed for a desired value of velocity, U_6 . At the same time, h_6 is larger for the real gas (equation 10, Appendix II) for equal initial values of the enthalpies, h_5 of the two gases (see figure 8), and correspondingly, P_6 is considerably larger for the real gas than for the ideal gas (see Figure 9). A more detailed discussion of these effects of γ on the real gas flow is presented by Yoler in Reference 5.

Because of the higher pressures and lower velocities in region 6 for the real gas, the resulting starting shock wave $(W_c)_r$ of the real gas is weaker than for the ideal gas (Figure 7). Conversely, the lower pressures and higher velocities in region 6 of the ideal gas result in a stronger starting shock wave $(W_c)_r$ for the ideal gas. The larger P_7/P_6 and U_6/U_7 across the stronger shock wave, $(W_c)_r$ of the ideal gas just compensate for the higher velocity, U_6 and lower pressure, P_6 of the ideal gas and, as shown in Figure 7, leads to the interesting result already mentioned, namely that the calculated predicted values of velocity, U_7/a_1 , and transmitted wave Mach number, M_{sd} are almost identically equal for the two gases, (ideal gas and equilibrium air). It should be mentioned here, though not shown on the graphs, that the values of the temperatures in regions 5 and 7 are considerably larger for the ideal gas than for the real gas in the corresponding regions.

Figure 7 also indicates that for the orifice area ratio A_6/A_* of 7.67, the values of M_6 for the real gas range from about 2.9 to 3.1 for M_{su} from 7.0 to 10. For these conditions the calculated values of Reynolds number in region 6 range from about 600 per inch at $M_{su} = 7.0$ to about 1200 per inch at $M_{su} = 10$ for initial shock tube pressure $P_1 = .40$ mm Hg and temperature $T_1 = 300^\circ\text{K}$.

IV. ORIFICE AND NOZZLE CONFIGURATIONS

Six configurations were investigated as shown in Figures 10a to 10f and as outlined below.

<u>Configuration</u>	<u>Type of Orifice</u>	<u>Shape and Size of Opening at Orifice Inlet</u>	<u>Area Ratio A_6/A_*</u>
A	wedge type	rectangular .375" x 2-7/8"	7.67
B	plate type	rectangular .375" x 2-7/8"	7.67
C	wedge type	rectangular .125" x 2-7/8"	23.0
D	plate type (sharp edge and round edge)	rectangular .125" x 2-7/8"	23.0
E	channel type	rectangular .125" x 2-7/8"	23.0
F	conical	round opening at inlet = .725" diameter opening at outlet = 2.0" diameter	7.67

Measurements were made of the strengths of the incident and transmitted shock waves for all of the above orifices, except for the channel type orifice E for which only schlieren photographs were made.

As shown in Figures 10a to 10f the inlet corners of the wedge and conical type orifices were machined smooth and round. The slight lack of symmetry of curvature at the inlets of the wedge type orifices which appears in the photographs of Figures 10a and 10c is purely an optical effect that results from trying to photograph the wedge

contours in a direction along the full $2\text{-}7/8$ " of vertical length of wedge. The actual curvatures at the inlets of the orifices investigated were symmetrical. For configuration D, measurements were made for both a sharp edge and a round edge orifice inlet, (Figures 10d₁ and 10d₂).

V. DISCUSSION OF RESULTS

A. Schlieren Studies

Schlieren photographs of the starting flow for two of the models investigated are shown in Figures 11 and 12. The values of time delay indicated on the above figures are measured from the time the incident shock wave reaches heat gage number 2, which is located at an arbitrary measured point just upstream of the face of the model investigated.

Figure 11 shows a sequence of consecutive photographs of the incident wave reflecting from the face of configuration E, the channel type orifice. The beginning of the transmitted wave can be seen in photograph number 11b. The unusual oblique wave configurations within the channel itself are indicated in photographs 11b to 11d.

In Figure 12 is shown a sequence of photographs of the starting flow and of the reflected and transmitted wave formation for configuration B, the plate type orifice. The dark regions at the edges of the throat of the orifice in photograph number 12b show the flow as it turns around the corner of the orifice beginning its expansion into region 6, until in photograph number 12c, in which the reflected wave has withdrawn sufficiently from the orifice opening, the orifice is flowing full. The progress and shape of the transmitted wave just downstream of the orifice are indicated very clearly in the sequence of photographs of Figure 12.

B. Measured Values of Transmitted Wave Speeds

1. Introductory Remarks

The values of the transmitted wave strengths, as indicated by the measured values of the Mach number M_{sd} , of the transmitted wave, are shown in Figures 13 to 17 for the various configurations investigated. Also in the above figures, the measured values of the transmitted wave speeds are compared with the predicted values of the wave speeds.

A brief inspection of each of the Figures 13 to 17 for orifice configurations A through F, shows that for some configurations the agreement was very good between measured and predicted values of transmitted wave Mach numbers, M_{sd} , whereas for other configurations the measured values of M_{sd} were less than those predicted, and for still other orifice configurations the measured values were greater than those predicted by the one-dimensional flow model.

These interesting differences between the configurations studied can be readily accounted for by an understanding of the flow process in the one-dimensional model, as discussed below. The general theory of the one-dimensional flow model was presented in Section III of this report. A detailed study of the stepwise calculations of this one-dimensional model shows that the measured value of M_{sd} for a particular configuration will be equal to, less than, or greater than the value of M_{sd} predicted by the one-dimensional theory, depending on whether the total pressure losses between regions 5 and 7 are respectively equal to, greater than, or less than those allowed for by the idealized

one-dimensional theory. The differences between actual and idealized total head losses result from boundary layer-shock wave interactions, oblique shock wave configurations rather than the idealized plane shock waves, and friction and eddy losses.

One other significant factor which could result in measured values of M_{sd} greater than those predicted by the one-dimensional theory is the case in which vena contracta effects at the sharp-edge orifice inlets produce an effective area, A_* , less than that of the geometrical measured area, A_6 , so that the resulting area ratio, A_6/A_* of the actual flow would be greater than that utilized in the one-dimensional calculations. (However, as discussed later in this section, no measurable vena contracta effects were present in the orifice models investigated).

On the basis of the foregoing introductory remarks regarding the factors influencing the magnitude of the transmitted wave Mach number, M_{sd} , the results of the investigation of each orifice configuration, A to F, are discussed individually below.

2. Configuration A, Wedge Type Orifice, Area Ratio $A_6/A_* = 7.67$

The results of the study at expansion chamber pressures of $P_1 = 5.0$ mm Hg and 14.0 mm Hg are shown in Figure 13. The agreement between the measured values of transmitted wave Mach number, M_{sd} and the predicted values based on the theoretical one-dimensional model for an ideal gas is remarkably good for the range of incident wave Mach number up to about $M_{su} = 4.3$. Beyond $M_{su} = 4.3$, although the agreement in the two values is still moderately good, the

measured values of transmitted wave speeds begin to depart slowly from the predicted values, possibly because as discussed earlier in this section under "Introductory Remarks", the general flow losses resulting from friction and turbulence may become significant at the higher values of Mach number, M_6 .

3. Configuration B, Plate-Type Orifice, Area Ratio $A_6/A_* = 7.67$

The measured values of the transmitted wave Mach numbers for configuration B are shown in Figure 14 for two ambient shock tube pressures, and are appreciably less than the predicted values. Again, this reduction in the measured values of M_{sd} as compared to predicted values may possibly be caused by the considerable eddy and turbulent losses in the flow resulting from the free expansion of the air from the orifice throat area, A_* to the area of region 6. The results of the measurements of configuration A and configuration B at the expansion chamber pressure, $P_1 = 5.0$ mm are compared in Figure 15.

4. Configuration C, Wedge-Type Orifice

Configuration D, Plate-Type Orifice, Sharp Edge

Configuration D, Plate-Type Orifice, Round Edge

(Area Ratio A_6/A_* for All 3 Orifices = 23)

Figure 16 indicates that the measured values of Mach number of the transmitted wave for configurations C and D are greater than those predicted by the idealized one-dimensional flow model. On the basis of the foregoing discussion, the flow losses through the shock wave configurations of the above orifices are less than those through the plane shock wave of the one-dimensional theory.

To observe the presence, if any, of vena contracta effects on the flow through the sharp edge orifice inlet, measurements were made with configuration D (plate-type free expansion orifice) for both sharp edge and round edge orifice inlets (Figures 10d₁ and 10d₂), and are presented in Figure 16. There was no significant measurable difference in the strength of the transmitted wave for the two types of edges (sharp and round) investigated, indicating no measurable vena contracta flow effects.

5. Configuration F, Conical Type Orifice, Area Ratio $A_6/A_* = 7.67$

For structural reasons, studies in the 2-7/8" x 2-7/8" shock tube were limited to an incident shock Mach number, M_{su} of about 6 because of the high pressures behind the reflected shock. Higher values of incident Mach number, M_{su} and considerably lower values of ambient pressure, P_1 can be attained in the 2-inch round shock tube than in the 2-7/8" x 2-7/8" tube in which the preceding configurations A through D were investigated. Therefore a new model, configuration F (Figure 10f), was prepared for use in the 2-inch round tube. The expansion area ratio A_6/A_* of this configuration F was equivalent to that of the wedge type configuration A, but the diverging section of configuration F was conical rather than a wedge.

a. Ambient Pressure, $P_1 = 2.5$ mm Hg

The measured values of the transmitted Mach number, M_{sd} at an ambient pressure $P_1 = 2.5$ mm Hg are shown in Figure 17 for configuration F, and are compared in that figure with the theoretically predicted values calculated for the one-dimensional flow model. The

agreement at this pressure between the measured and predicted values is remarkably good for the full range of incident Mach numbers investigated (M_{su} of 4.1 to 7.1). The small observed differences possibly result from friction and eddy flow losses. The flow through the nozzle at this pressure of $P_1 = 2.5$ mm Hg appears to be rather satisfactorily established as indicated by the relatively moderate amount of scatter in the values of the measured data. It is also of interest that the measured values of transmitted wave speeds for the wedge type orifice, configuration A (at $P_1 = 5.0$ mm Hg) and the conical type orifice, configuration F (at $P_1 = 2.5$ mm Hg) are in excellent agreement for the range of M_{su} investigated.

b. Ambient Pressure, $P_1 = 0.4$ mm Hg

The effect of reducing the ambient tube pressure to 0.4 mm Hg is also shown in Figure 17. The scatter of the data at this lower pressure is considerably greater than for any other measurements or configurations discussed in this report. Inasmuch as the accuracy of the measuring technique is not affected by the low pressures in the tube, this wide scatter of the measured data at these low pressures is believed to be related to the flow itself. Also, at this low value of ambient tube pressure the agreement between measured and predicted values of M_{sd} is poor, the measured values of transmitted wave speeds being considerably greater than those predicted by the one-dimensional theory. At this low pressure it is likely that the boundary layer thickness behind the transmitted shock wave is so large that the flow downstream of the orifice does not expand to the full geometrical area of region 6. In that case the starting shock wave configuration, $(W_c)_r$

is weaker and the transmitted wave is correspondingly stronger than that predicted by the one-dimensional flow model. It is also quite likely that the starting shock wave configuration of the actual flow is a system of oblique shock waves rather than the plane wave of the idealized flow model.

VI. CONCLUDING REMARKS

1. The one-dimensional flow model discussed in this report yields a satisfactory prediction of the speed of the shock transmitted through the orifice. Depending on whether the flow losses through the starting shock wave configuration are greater than or less than those postulated in the plane wave of the one-dimensional model, the measured values of the transmitted wave Mach number will correspondingly be lower or higher.

2. For the range of incident shock Mach numbers investigated in this report, the calculated values of transmitted wave Mach number for an ideal gas and for equilibrium air are almost identical at an area ratio, $A_6/A_* = 7.67$, even though the velocities, temperatures, and pressures in the intermediate flow regions are quite different for the two gases (ideal gas and real gas).

3. This investigation suggests the desirability of further studies with larger area ratios A_6/A_* , particularly with the conical orifice, and also at lower ambient shock tube pressures.

REFERENCES

1. Rabinowicz, J.: Aerodynamic Studies in the Shock Tube. GALCIT Hypersonic Research Project, Memorandum No. 38, June 10, 1957.
2. Glick, H. S.; Hertzberg, A.; and Smith, W. E.: Flow Phenomena in Starting a Hypersonic Shock Tunnel. Cornell Aeronautical Laboratory, Report No. AD-789-A-3, (AEDC-TN-55-16), March, 1955.
3. Feldman, S.: Hypersonic Gas Dynamic Charts for Equilibrium Air. AVCO Research Laboratory, January, 1957.
4. Franks, W. J.: Interaction of a Shock Wave with a Wire Screen. Institute of Aerophysics, University of Toronto, UTIA Technical Note No. 13, May, 1957.
5. Yoler, Y. A.: Hypersonic Shock Tube. GALCIT Hypersonic Research Project, Memorandum No. 18, July 19, 1954.
6. Glass, I. I.; Martin, W.; and Patterson, G. N.: A Theoretical and Experimental Study of the Shock Tube. Institute of Aerophysics, University of Toronto, UTIA Report No. 2, November, 1953.

APPENDIX I

OUTLINE OF PROCEDURE FOR CALCULATING THE PREDICTED
VALUES OF THE TRANSMITTED WAVE SPEEDS, M_{sd} , FOR AN
IDEAL GAS BASED ON THE THEORETICAL ONE-DIMENSIONAL
MODEL DESCRIBED IN THIS REPORT *

Region 2

For specified initial conditions in the shock tube, the conditions in region 2 (Figure 3) behind the incident shock wave are described by the following equations.

$$\frac{P_2}{P_1} = 1 + \frac{2\gamma}{\gamma+1} (M_{su}^2 - 1) \quad (1)$$

$$\left(\frac{a_2}{a_1}\right)^2 = 1 + \frac{2(\gamma-1)}{(\gamma+1)^2} \left[\gamma M_{su}^2 - \frac{1}{M_{su}^2} - (\gamma-1) \right] \quad (2)$$

$$\frac{U_2 - U_1}{a_1} = \frac{2}{\gamma+1} \left(M_{su} - \frac{1}{M_{su}} \right) \quad (3)$$

$$\frac{\rho_2}{\rho_1} = \frac{\gamma+1}{\gamma-1 + \frac{2}{M_{su}^2}} \quad (4)$$

* Note: The stepwise procedure for the ideal gas calculation is described in some detail in this appendix because a similar stepwise procedure identical in principle (but different flow equations) is used in the calculation of the wave speeds of the real gas one-dimensional model described in Appendix II.

Region 5

Similarly, the conditions in region 5 behind the reflected shock wave are described by the equations,

$$\frac{P_5}{P_2} = 1 + \frac{2\gamma}{\gamma+1} \left[M_{s2}^2 - 1 \right] \quad (5)$$

$$\frac{U_5 - U_2}{a_2} = - \frac{2}{\gamma+1} \left[M_{s2} - \frac{1}{M_{s2}} \right] \quad (6)$$

$$\left(\frac{a_5}{a_2} \right)^2 = \frac{2(\gamma-1)}{(\gamma+1)^2} \left[\gamma M_{s2}^2 - \frac{1}{M_{s2}^2} - (\gamma-1) \right] + 1 \quad (7)$$

$$\frac{P_5}{P_2} = \frac{1}{1 - \frac{2}{\gamma+1} \left(1 - \frac{1}{M_{s2}^2} \right)} \quad (8)$$

$$\left(\frac{A_5}{A_*} \right)^{\frac{2(\gamma-1)}{\gamma+1}} = \frac{1}{\left(\frac{U_5}{a_5} \right)} \left[\frac{1 + \frac{\gamma-1}{2} \left(\frac{U_5}{a_5} \right)^2}{1 + \frac{\gamma-1}{2}} \right] \quad (9)$$

The preceding equations 5 to 9 would ordinarily be solved by an iteration process because the velocity U_5 behind the reflected wave is not known, inasmuch as there is some mass flow through the orifice opening. However, it was determined by several preliminary calculations that for the small area ratios A_*/A_5 of the orifices involved, the effect of the very small value of U_5 on the subsequent values of M_{sd} was negligibly small, and so subsequent calculations were made for the boundary condition $U_5 = 0$.

For the boundary condition $U_5 = 0$ (and $U_1 = 0$), M_{s2} can be eliminated from the preceding equations 5 to 9 and conditions in region 5 behind the reflected shock wave can be described by the equations (see Reference 6)

$$\frac{P_5}{P_2} = \frac{\left(1 + 2 \frac{\gamma - 1}{\gamma + 1}\right) \frac{P_2}{P_1} - \frac{\gamma - 1}{\gamma + 1}}{\frac{\gamma - 1}{\gamma + 1} \frac{P_2}{P_1} + 1} \quad (10)$$

$$\left(\frac{a_5}{a_2}\right)^2 = \frac{T_5}{T_2} = \frac{\frac{P_5}{P_2} \left(\frac{\gamma + 1}{\gamma - 1} + \frac{P_5}{P_2}\right)}{1 + \left(\frac{\gamma + 1}{\gamma - 1}\right) \frac{P_5}{P_2}} \quad (11)$$

Region 6

Conditions in region 6 can be calculated from the conditions in region 5 (which can be considered as a stagnation region) by means of an isentropic expansion to the full area of region 6, thereby determining M_6 , A_6 , P_6 , and U_6 .

Region 8

In this investigation the initial conditions in region 9 are equal to those in region 1, and are therefore specified in advance, so the conditions in region 8 are determined entirely by the Mach number of the transmitted wave, M_{sd} . The pressures and velocities in region 8 are therefore determined by the equations,

$$\frac{P_8}{P_9} = 1 + \frac{2\gamma}{\gamma+1} \left(M_{sd}^2 - 1 \right) = \frac{P_8}{P_1} \quad (12)$$

$$\frac{U_8 - U_9}{a_9} = \frac{2}{\gamma+1} \left(M_{sd} - \frac{1}{M_{sd}} \right) = \frac{U_8}{a_1} \quad (13)$$

(In above equation 13, $a_9 = a_1$, and $U_9 = 0$ in this report.)

Region 7

Similarly to the above, for the flow conditions in region 8 determined earlier, the conditions in region 7 are determined solely by the magnitude of the Mach number of the starting shock wave $(M_c)_r$. The pressures and velocities in region 7 are therefore determined by the equations

$$\frac{P_7}{P_6} = 1 + \frac{2\gamma}{\gamma+1} \left[(M_c)_r^2 - 1 \right] \quad (14)$$

$$\frac{P_7}{P_1} = \frac{P_7}{P_6} \cdot \frac{P_6}{P_1} \quad (15)$$

$$\frac{U_7 - U_6}{a_6} = -\frac{2}{\gamma+1} \left[(M_c)_r - \frac{1}{(M_c)_r} \right] \quad (16)$$

but U_6/a_6 is already known from the conditions in region 6,

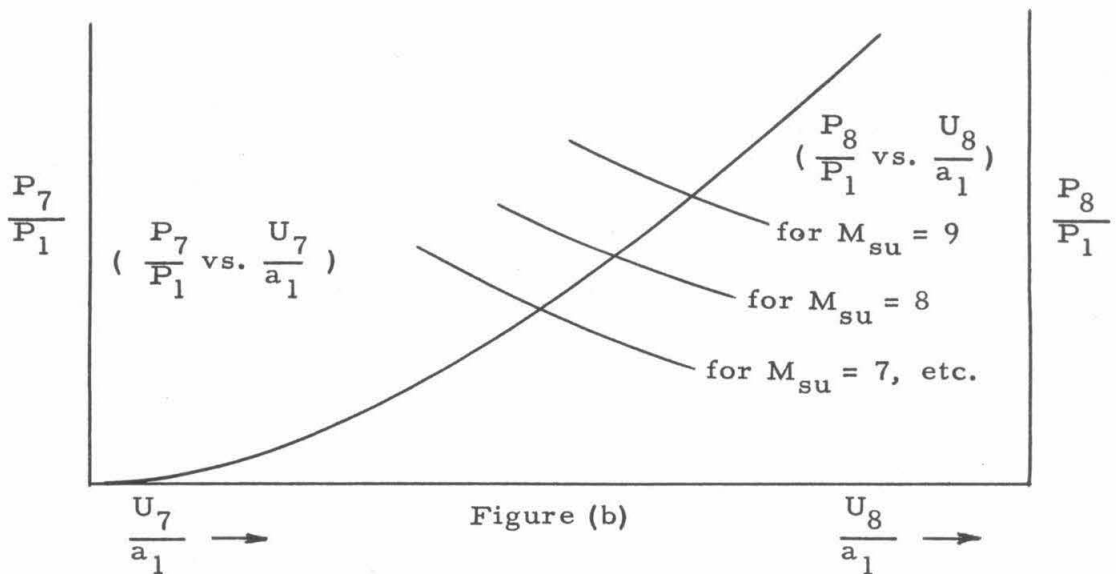
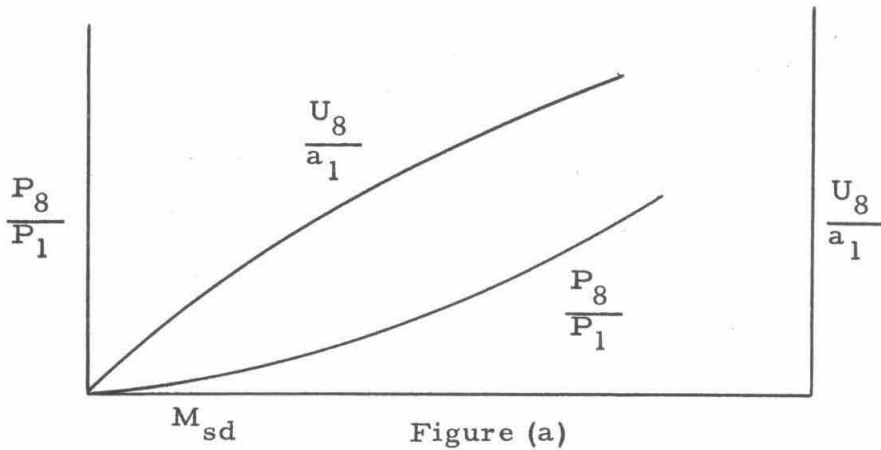
$$\therefore \frac{U_7}{a_6} = -\frac{2}{\gamma+1} \left[(M_c)_r - \frac{1}{(M_c)_r} \right] + \frac{U_6}{a_6} \quad (17)$$

and

$$\frac{U_7}{a_1} = \frac{U_7}{a_6} \cdot \frac{a_6}{a_1} \quad (18)$$

Matching of Velocities and Pressures of Regions 7 and 8

By means of a relatively easy graphical procedure, one determines M_{sd} by matching P_8/P_1 and U_8/a_1 (of equations 12 and 13) with P_7/P_1 and U_7/a_1 (of equations 15 and 18) inasmuch as the velocities and pressures are equal across the contact surface. The above matching of velocities and pressures is very conveniently accomplished as shown in the figures below.



The graph of P_8/P_1 and U_8/a_1 shown in preceding Figure (a) is calculated from equations 12 and 13 for a range of transmitted wave Mach numbers, M_{sd} .

The graph of P_8/P_1 vs. U_8/a_1 in the preceding Figure (b) is a cross-plot of Figure (a) with incident values of M_{su} as parameter.

Then for an arbitrary specified value of M_{su} , one solves equations 15 and 18 for several assumed values of $(M_c)_r$ and draws the graph of P_7/P_1 vs. U_7/a_1 on the same Figure (b).

The intersection of the above 2 graphs in Figure (b) yields the values of P_8/P_1 and U_8/a_1 , which correspond to the desired value of M_{sd} for the value of M_{su} specified.

APPENDIX II

OUTLINE OF PROCEDURE FOR CALCULATING THE PREDICTED
VALUES OF THE TRANSMITTED WAVE SPEEDS, M_{sd} ,
IN EQUILIBRIUM AIR BASED ON THE THEORETICAL
ONE-DIMENSIONAL MODEL DESCRIBED IN THIS REPORT

Region 2

For the particular case of initial shock tube temperature $T_1 = 300^\circ\text{K}$, the conditions in regions 2 and 5 are shown for equilibrium air on a very convenient set of charts in Reference 3 for a wide range of initial shock tube pressures, P_1 .

Region 5

In region 5 the velocity U_5 behind the reflected wave is not strictly $= 0$. However, as was done for the case of an ideal gas discussed in Appendix I, for the small area ratios A_*/A_5 investigated, the effect of the small velocities, U_5 , on the resultant value of M_{sd} is negligibly small, and so in all subsequent calculations of M_{sd} in this report the value of U_5 is assumed $= 0$. Conditions in region 5 behind the reflected shock wave are shown in the charts of Reference 3.

Region 6

The expansion from region 5 to region 6 was considered as isentropic. So accordingly,

$$S_5 = S_6 \quad (\text{constant entropy}) \quad (1)$$

$$h_6 + \frac{U_6^2}{2} = h_5 + \frac{U_5^2}{2} \quad (2)$$

and neglecting the extremely small effect of U_5 as discussed earlier,

$$U_6^2 = 2(h_5 - h_6) \quad (3)$$

$$U_*^2 = 2(h_5 - h_*) \quad (4)$$

To determine the enthalpy, h_6 , in region 6, one must first determine the density or pressure in region 6.

The density in region 6 was determined by an iteration method by which one first determines the mass flow through the orifice as follows:

$$S_5 = S_* = S_6 \quad (5)$$

(S_5 is known from the earlier calculated conditions in region 5)

$$U_* = a_* \quad (6)$$

A value of h_* is assumed.

Then, for the above values of h_* and S_* one determines a_* and ρ_* from the Mollier diagram.

Also, for the above value of h_* , and the already known value of h_5 , one calculates U_* from equation 4.

One continues to select values of h_* until the condition $U_* = a_*$ of equation 6 is satisfied.

$$\text{Therefore } \rho_* U_* A_* \text{ is known.} \quad (7)$$

But from the equation of conservation of mass,

$$\rho_* U_* A_* = \rho_6 U_6 A_6 \quad (8)$$

$$\text{Now one assumes (guesses) a value of } h_6. \quad (9)$$

From the Mollier diagram, for the above h_6 and the known value of S_6 (equation 5), one determines a corresponding value of ρ_6 . (10)

Also, for the above assumed value of h_6 one calculates a corresponding value of U_6 by means of equation 3. (11)

The values of ρ_6 and U_6 from equations 10 and 11 together with the known value of the area A_6 , are compared with the known mass flow $\rho_* U_* A_*$ as shown in equation 8 above.

One continues to select values of h_6 as per equation 17 until the corresponding values of ρ_6 and U_6 determined from equations 10 and 11 satisfy the mass flow equation 8. So now conditions in region 6 are known.

Region 8

The pressure ratios P_8/P_9 and velocity ratio $(U_8 - U_9)/a_9$ across the transmitted shock wave are calculated in a manner similar to that for region 2, i. e., for $P_9 = P_1$, $U_9 = 0$, and $T_9 = 300^\circ\text{K}$. Conditions in region 8 can be determined from the charts of Reference 3.

Region 7

The conditions in region 7 are calculated directly from the equations of motion for a moving shock wave, i. e.,

$$\frac{U_7 - U_6}{a_6} = \left[\frac{(W_c)_r}{a_6} \right] \left[1 - \frac{\rho_6}{\rho_7} \right] \quad (12)$$

$$P_7 = P_6 + \left[\rho_6 a_6^2 \right] \left[\frac{(W_c)_r}{a_6} \right]^2 \left[1 - \frac{\rho_6}{\rho_7} \right] \quad (13)$$

$$h_7 = h_6 + \left[\frac{1}{2} a_6^2 \right] \left[\frac{(W_c)_r}{a_6} \right]^2 \left[1 - \frac{p_6^2}{p_7^2} \right] \quad (14)$$

Equation of state of gas is described by the Mollier diagram of Reference 3. (15)

It should be noted that in the preceding equations 12 to 14, the expression $(W_c)_r$ is the speed of the starting compression wave relative to the fluid into which it is advancing, i. e., relative to the velocity U_6 in region 6.

Matching of Velocities and Pressures of Regions 7 and 8

The technique and procedure for matching the pressures and velocities of regions 7 and 8 (i. e., across the contact surface) are identical to that described in Appendix I for the ideal gas, except, of course, that in the case of the real gas discussed here in Appendix II, for each assumed value of $(W_c)_r/a_6$ in equations 12 to 14, the quantities P_7/P_1 and U_7/a_1 must be calculated by an iteration procedure. The proper matching of the pressures and velocities in regions 7 and 8 in accordance with the procedure referred to above, yields the desired values of M_{sd} in equilibrium air for the particular value of M_{su} specified.

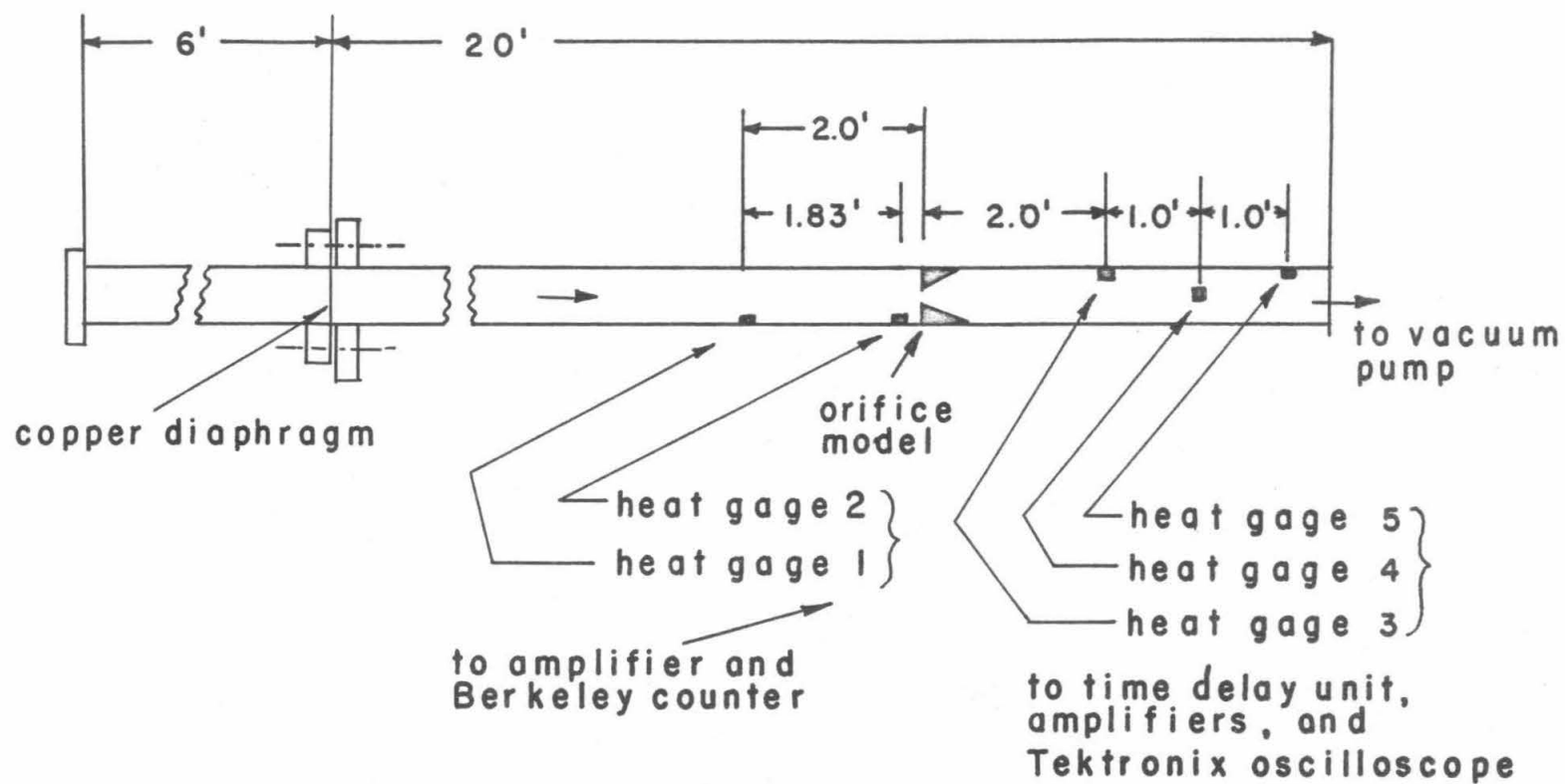
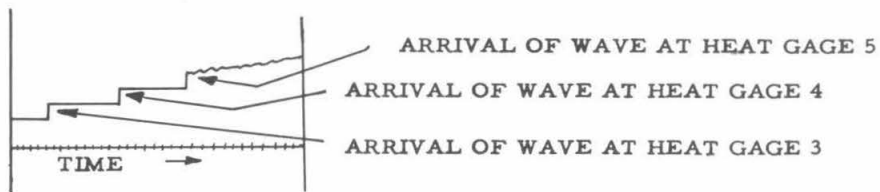
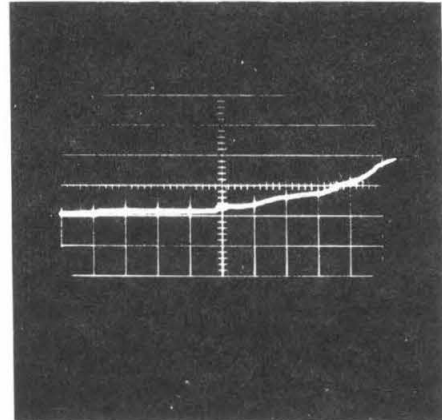
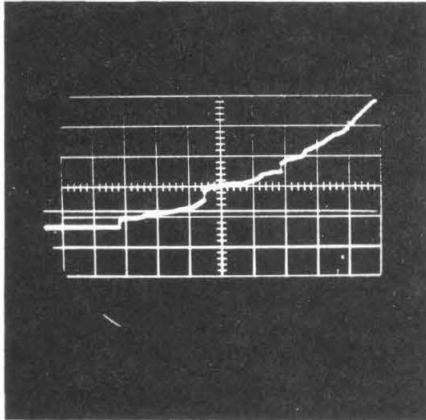


FIGURE 1
TYPICAL MODEL INSTALLATION IN 2-7/8" x 2-7/8" SHOCK
TUBE SHOWING LOCATION OF MODEL AND HEAT GAGES



TYPICAL INTERPRETATION OF ABOVE OSCILLOSCOPE PHOTOGRAPHS

SWEEP, MICROSECONDS PER CM = 100

SENSITIVITY, MILLIVOLTS PER CM = 5

FIGURE 2
TYPICAL OSCILLOSCOPE RECORDS FOR
MEASURING THE TRANSMITTED WAVE SPEED

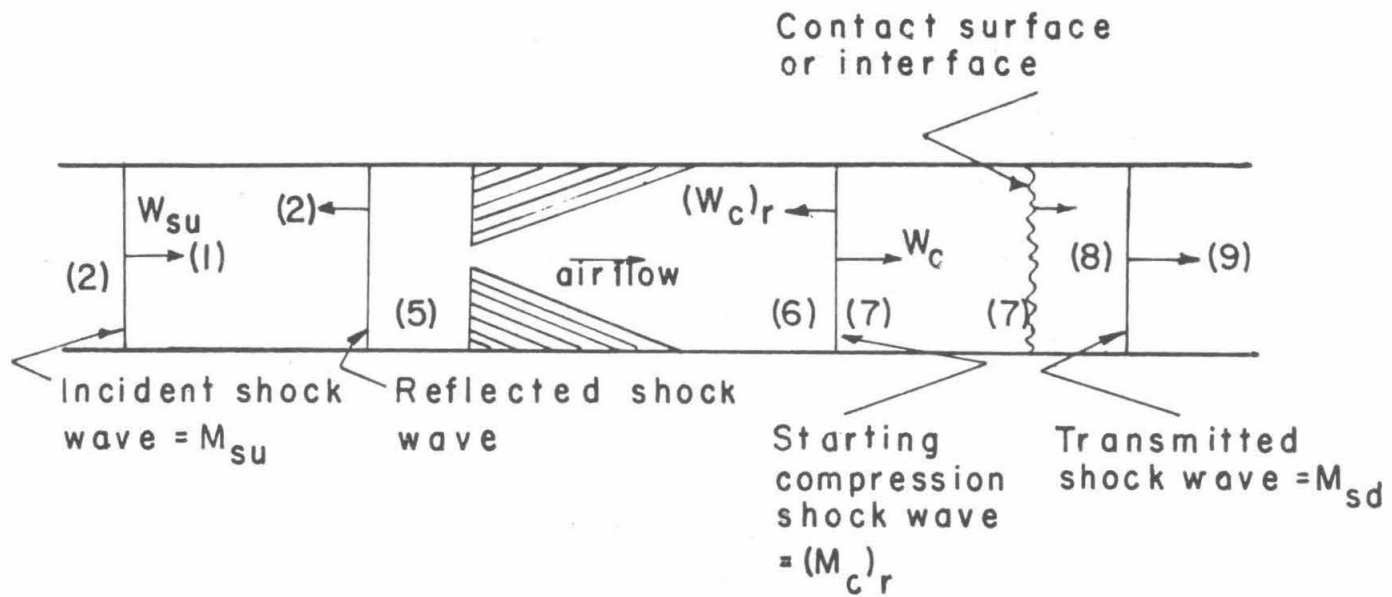


FIGURE 3

SCHEMATIC OF FLOW REGIONS

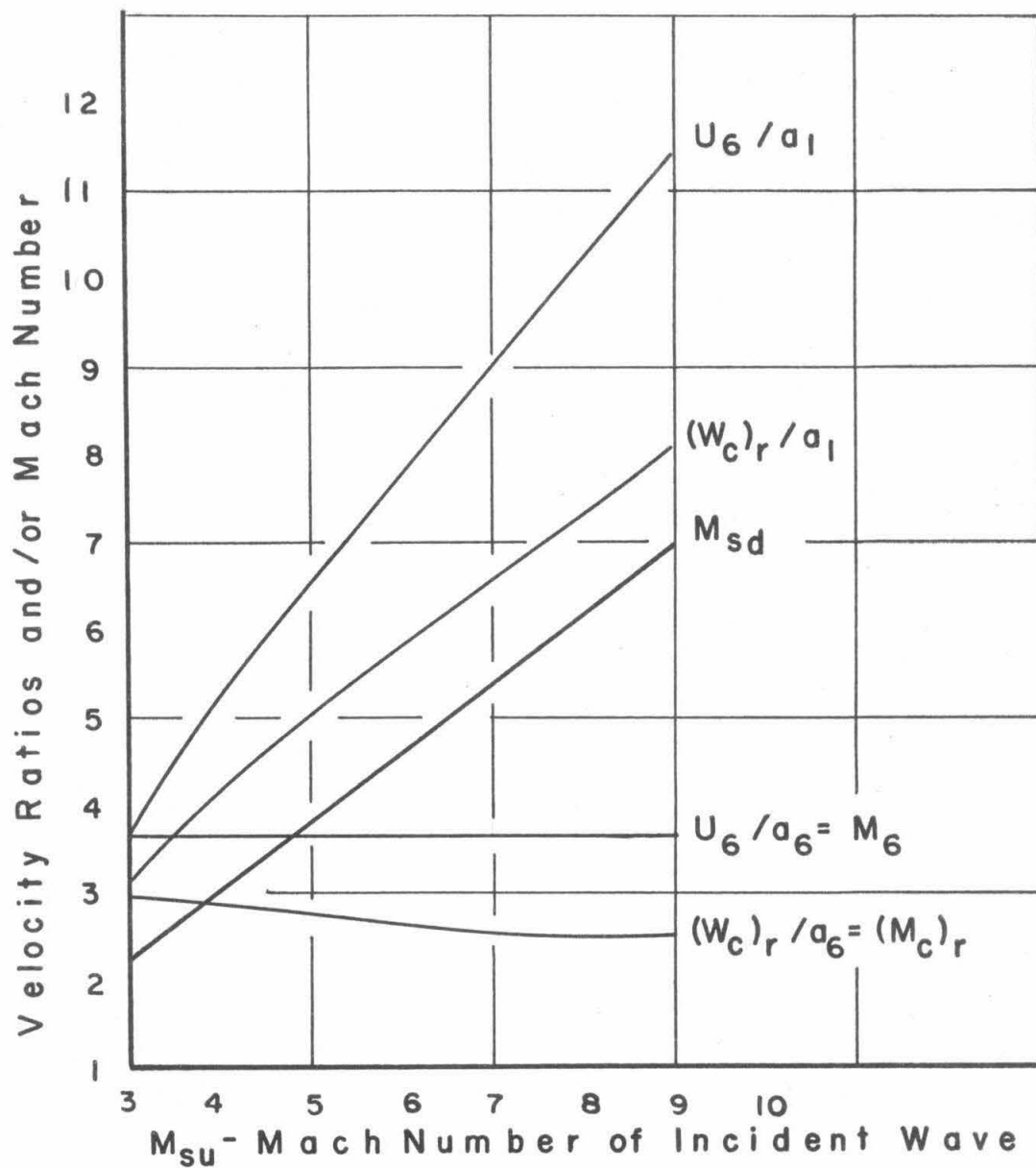


FIGURE 4

CALCULATED VALUES OF VELOCITY RATIOS AND MACH NUMBERS BASED ON THEORETICAL ONE DIMENSIONAL MODEL FOR IDEAL GAS ($\gamma = 1.40$), AREA RATIO $A_6/A_* = 7.67$

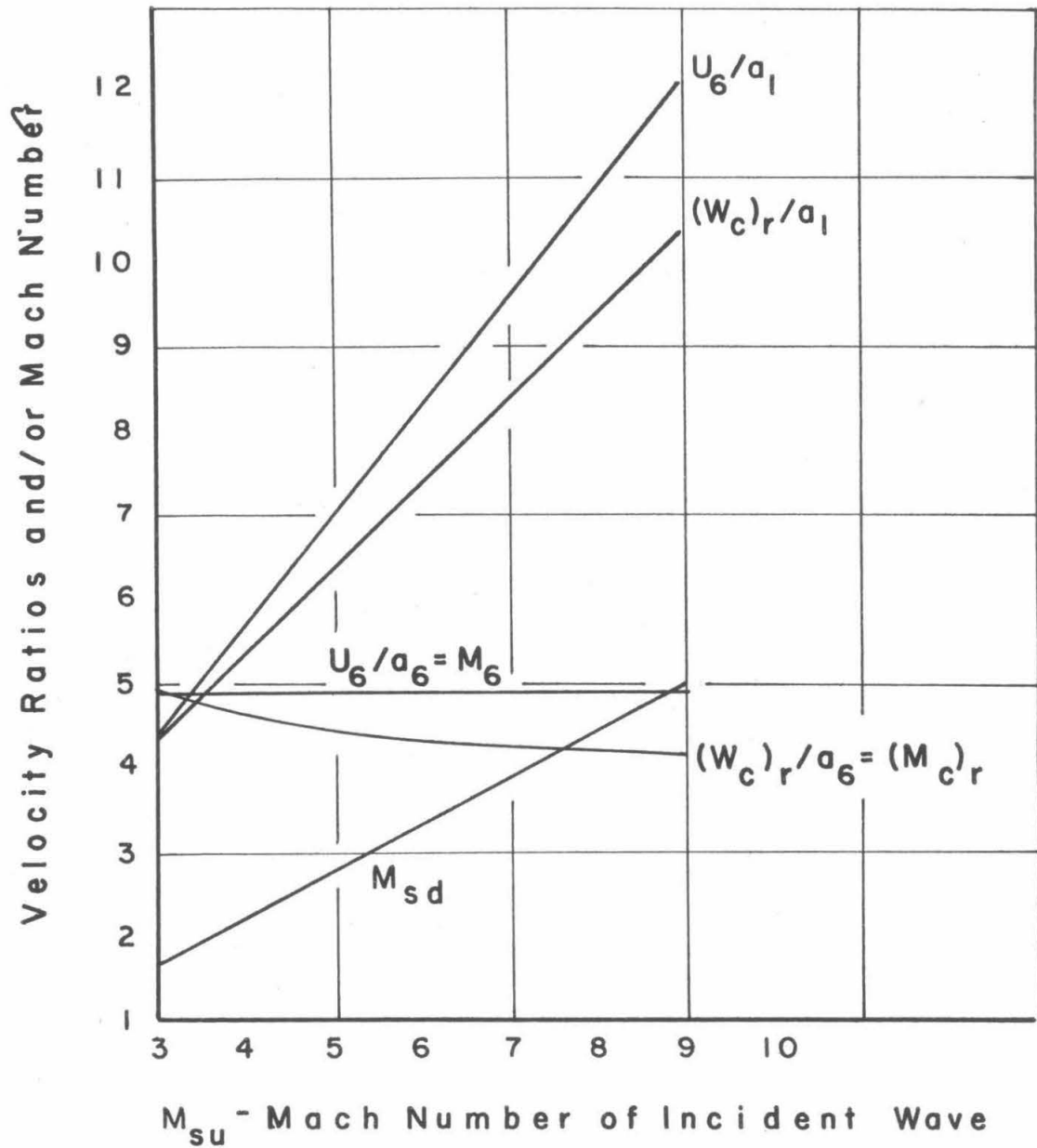


FIGURE 5
CALCULATED VALUES OF VELOCITY RATIOS AND MACH
NUMBERS BASED ON THEORETICAL ONE DIMENSIONAL
MODEL FOR IDEAL GAS ($\gamma = 1.40$), AREA RATIO $A_6/A_* = 23.0$

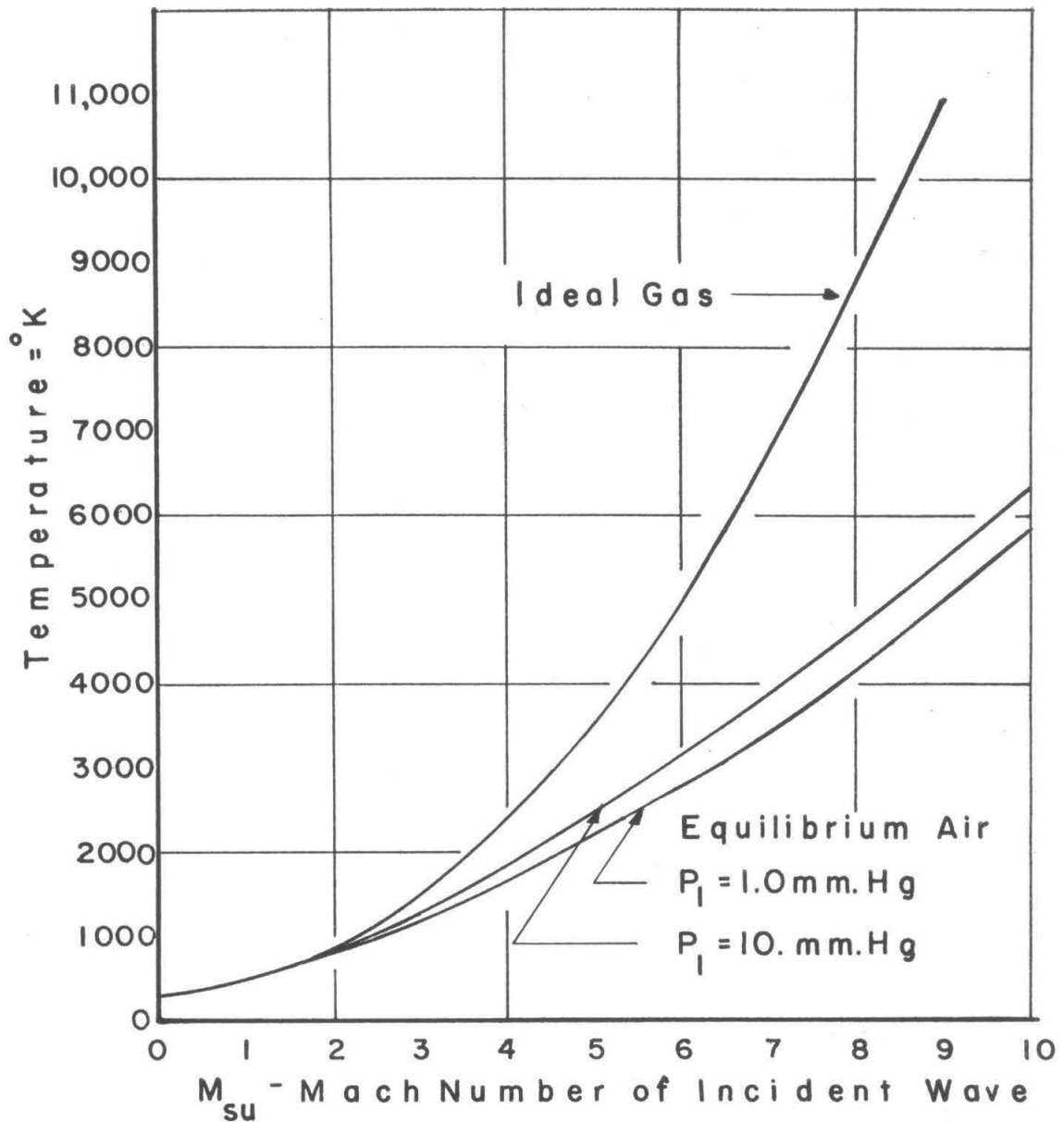


FIGURE 6
TEMPERATURES IN REGION 5 BEHIND THE REFLECTED
SHOCK WAVE FOR IDEAL GAS AND REAL GAS.
AMBIENT SHOCK TUBE TEMPERATURE $T_1 = 300^\circ\text{K}$

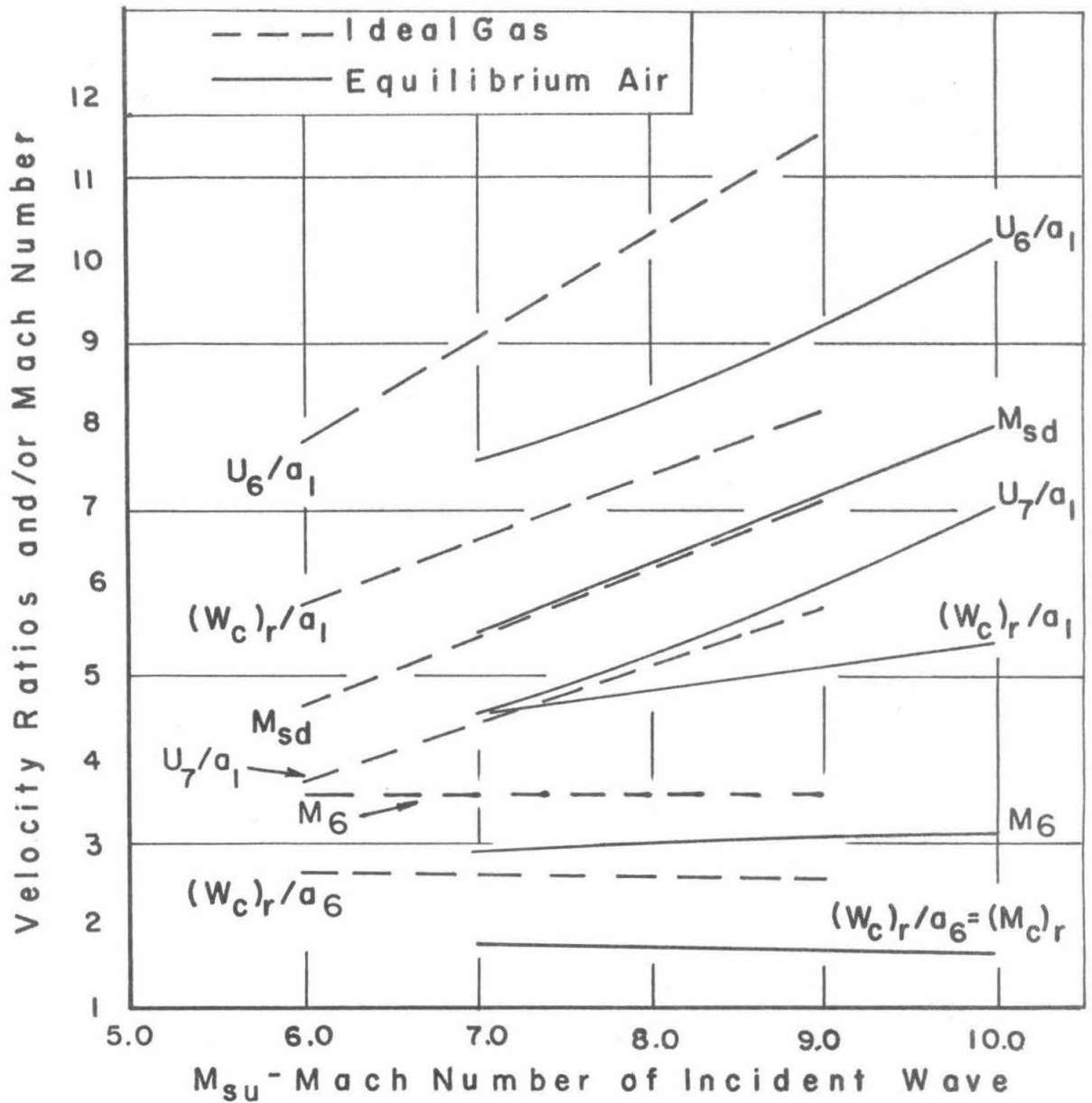


FIGURE 7

CALCULATED VALUES OF VELOCITY RATIOS AND MACH NUMBERS BASED ON THEORETICAL ONE DIMENSIONAL FLOW MODEL FOR EQUILIBRIUM AIR AND FOR IDEAL GAS ($\gamma = 1.40$), AREA RATIO $A_6/A_* = 7.67$

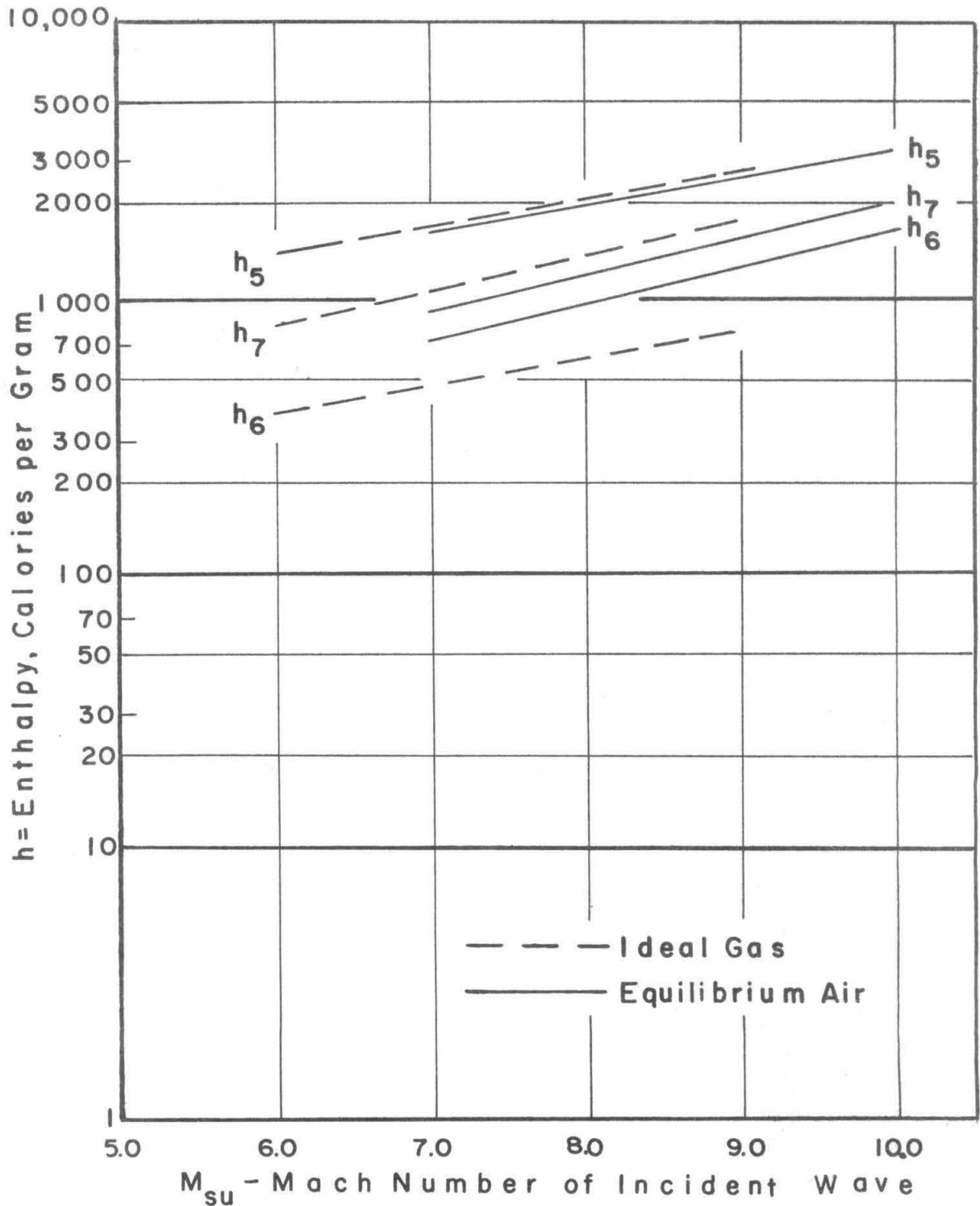


FIGURE 8

CALCULATED VALUES OF ENTHALPY IN FLOW REGIONS 5, 6, AND 7 BASED ON THEORETICAL ONE DIMENSIONAL FLOW MODEL FOR EQUILIBRIUM AIR AND FOR IDEAL GAS ($\gamma = 1.40$), AREA RATIO $A_0/A_* = 7.67$

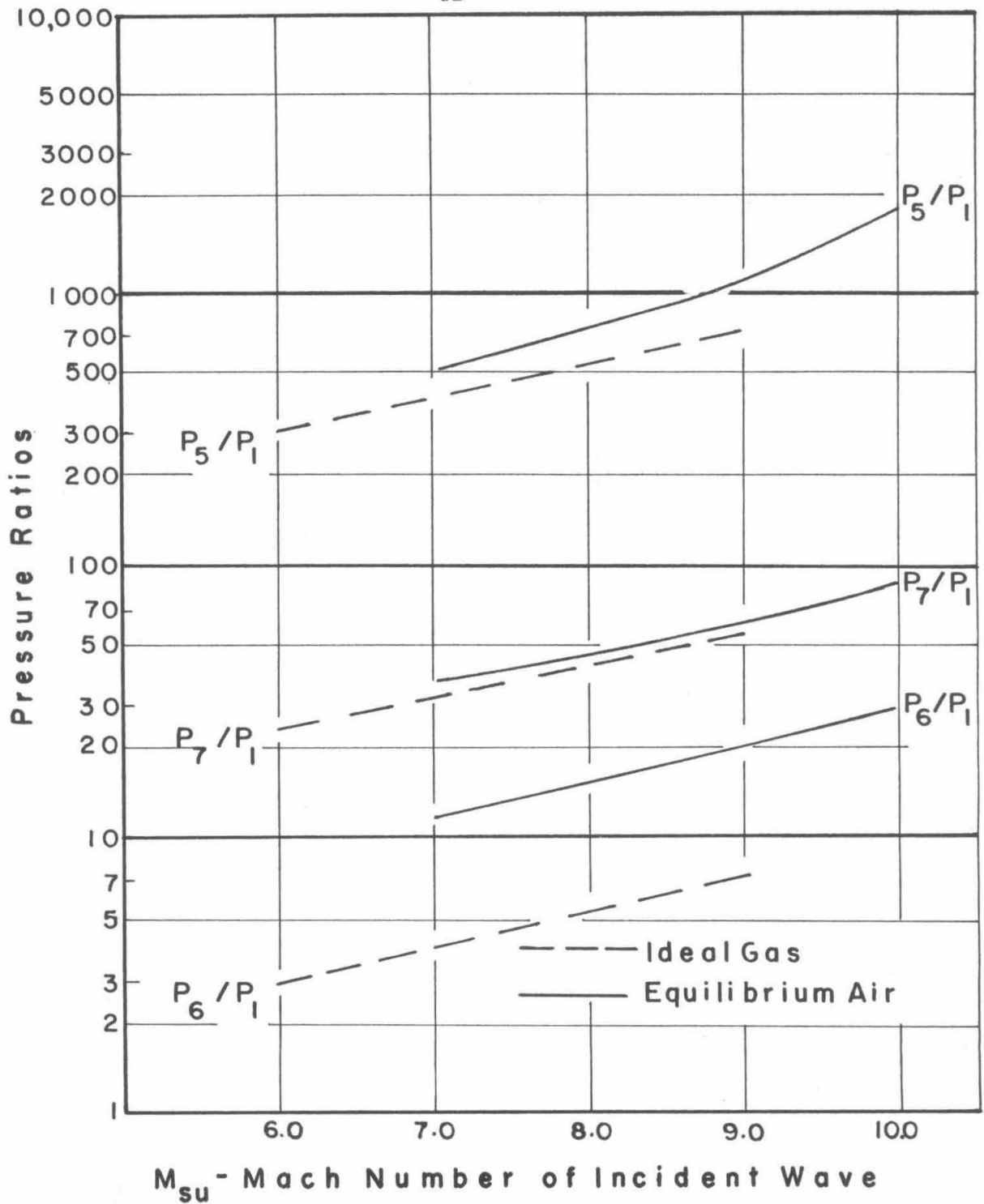


FIGURE 9

CALCULATED VALUES OF PRESSURE RATIOS IN FLOW REGIONS 5, 6, AND 7 BASED ON THEORETICAL ONE DIMENSIONAL FLOW MODEL FOR EQUILIBRIUM AIR AND FOR IDEAL GAS ($\gamma = 1.40$), AREA RATIO $A_0/A_* = 7.67$

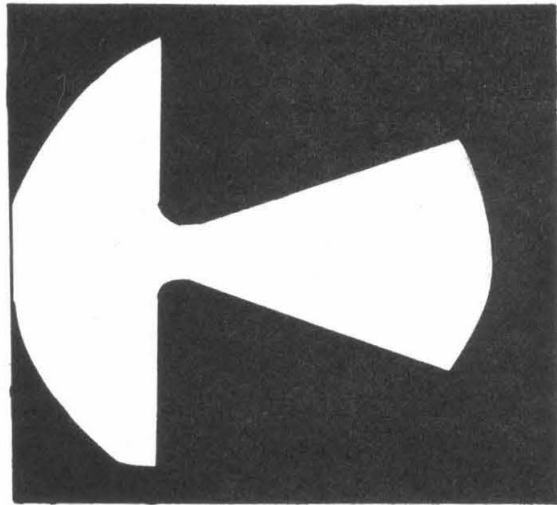
Configuration A -
Wedge type orifice

Orifice opening
= .375" x 2.875"

Direction of airflow →

Area ratio $A_6/A_* = 7.67$

Semi-divergent angle
of wedge = $19^\circ - 50'$



(a)

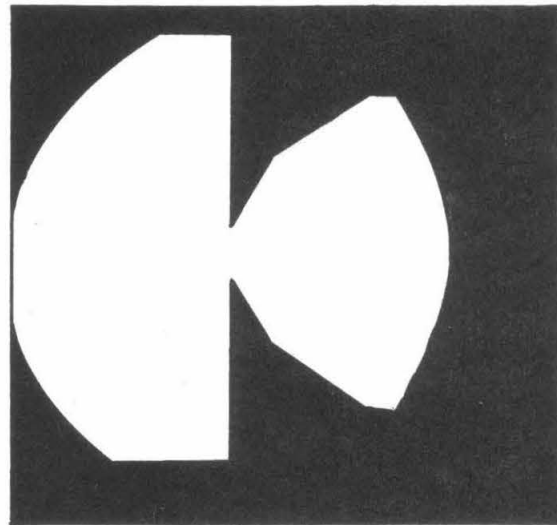
Configuration B -
Plate type orifice

Orifice opening
= .375" x 2.875"

Direction of airflow →

Area ratio $A_6/A_* = 7.67$

Semi-divergent angle = 60°



(b)

Figure 10 - Photographs and sketches of profile of flow passage through orifices as seen through viewing opening in shock tube.

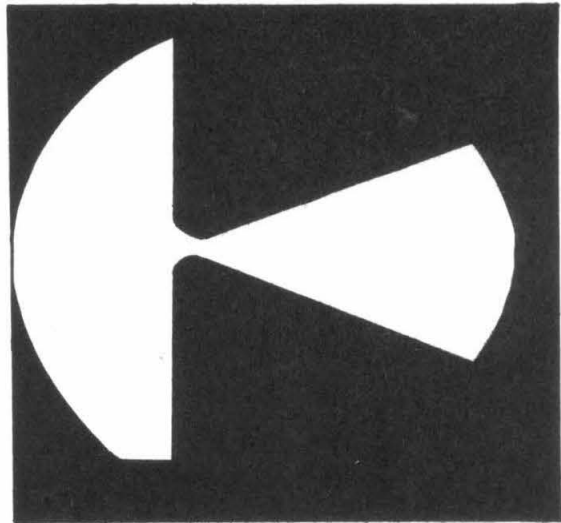
Configuration CWedge type orifice

Orifice opening
 $= .125'' \times 2.875''$

Direction of airflow \longrightarrow

Area ratio $A_6/A_* = 23.0$

Semi-divergent angle
 of wedge $= 21^\circ - 30'$



(c)

Configuration D(sharp edge)Plate type orifice

Orifice opening
 $= .125'' \times 2.875''$

Direction of airflow \longrightarrow

Area ratio $A_6/A_* = 23.0$

Semi-divergent angle $= 60^\circ$

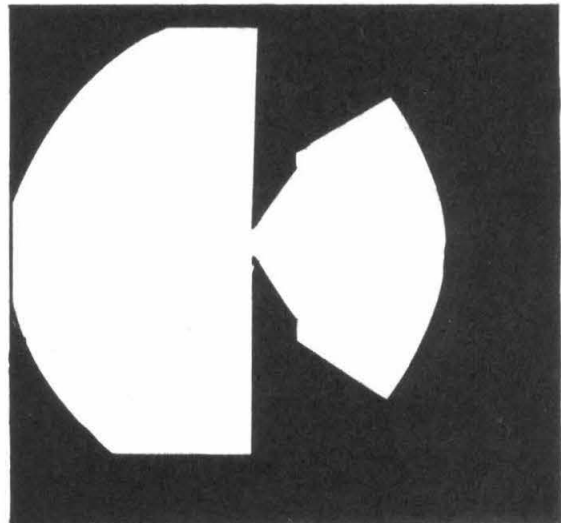
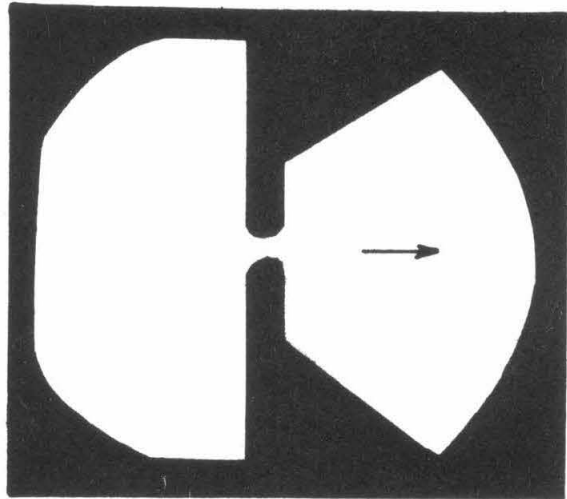
(d₁)

Figure 10 - (continued) - Photographs and sketches of profile of flow passage through orifices as seen through viewing opening in shock tube.

Configuration D(round edge)Plate type orifice

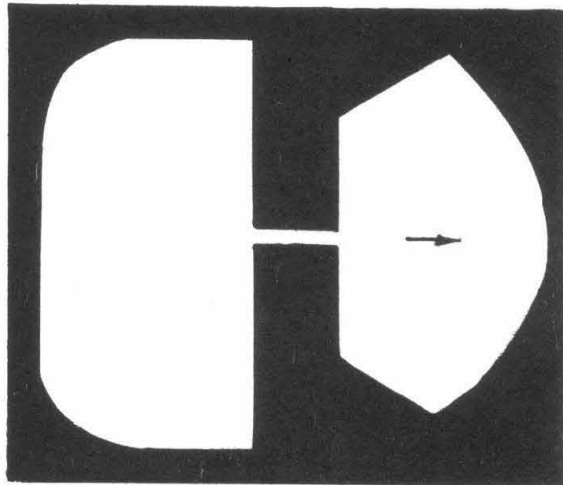
Direction of airflow →

Orifice opening

 $= .125'' \times 2.875''$ Area ratio $A_6/A_* = 23.0$ (d₂)Configuration EChannel type orifice

Direction of airflow →

Orifice opening

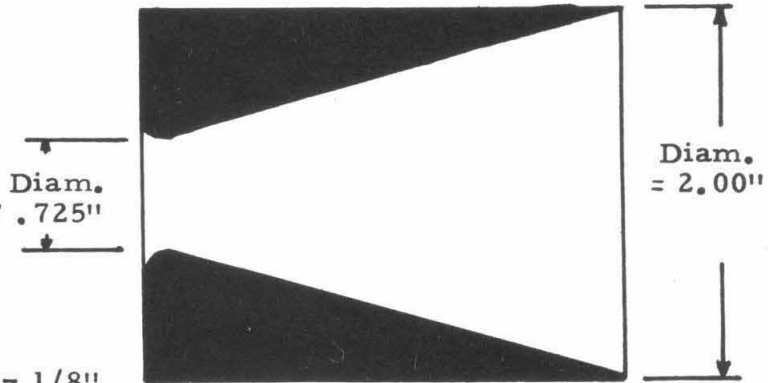
 $= .125'' \times 2.875''$ Area ratio $A_6/A_* = 23.0$ 

(e)

Figure 10 - (continued) - Photographs and sketches of profile of flow passage through orifices as seen through viewing opening in shock tube.

Configuration FConical type orifice

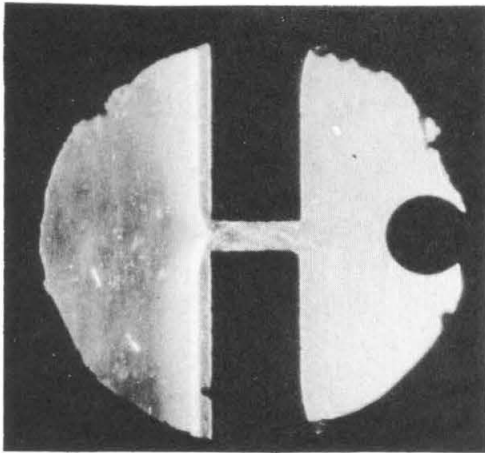
Direction of airflow →

Area ratio $A_6/A_* = 7.67$.725"Semi-divergent angle
of cone = 14° Radius of lip of orifice = $1/8$ "

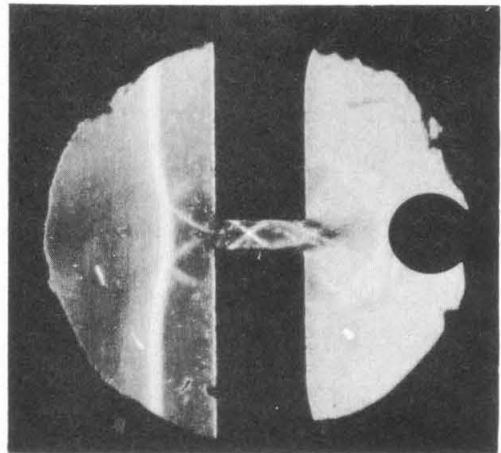
(f)

Sectional view of conical type orifice

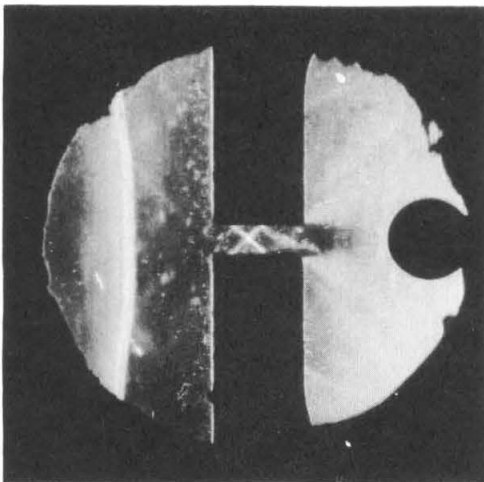
Figure 10 - (continued) - Photographs and sketches of profile of flow passage through orifices as seen through viewing opening in shock tube.



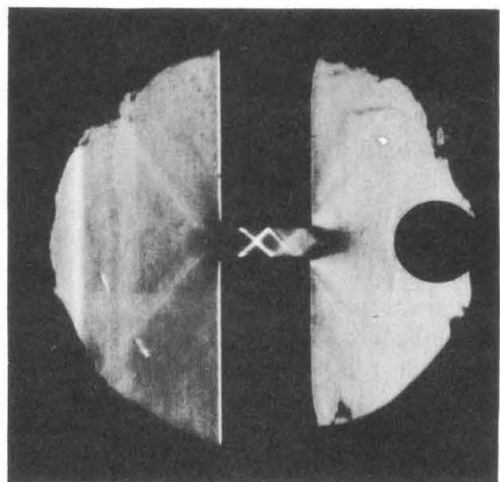
(a)
TIME DELAY = 20 MICROSECONDS



(b)
TIME DELAY = 30 MICROSECONDS

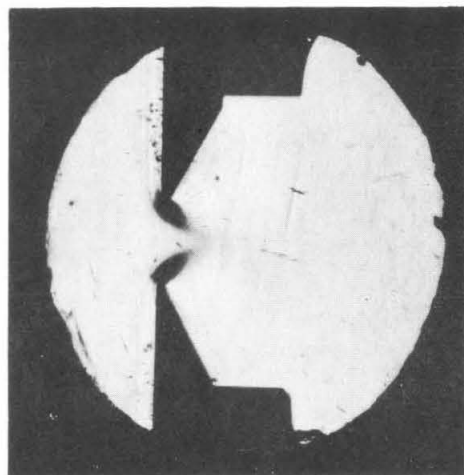


(c)
TIME DELAY = 35 MICROSECONDS



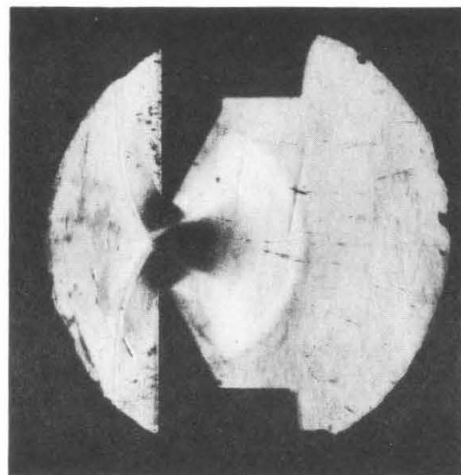
(d)
TIME DELAY = 50 MICROSECONDS

FIGURE 11
CONFIGURATION E, CHANNEL TYPE ORIFICE, SEQUENCE OF
SCHLIEREN PHOTOGRAPHS SHOWING THE INCIDENT WAVE
REFLECTING FROM THE FACE OF THE MODEL, AND ALSO
THE SUBSEQUENT WAVES. $M_{su} = 5.0$ (APPROXIMATELY)



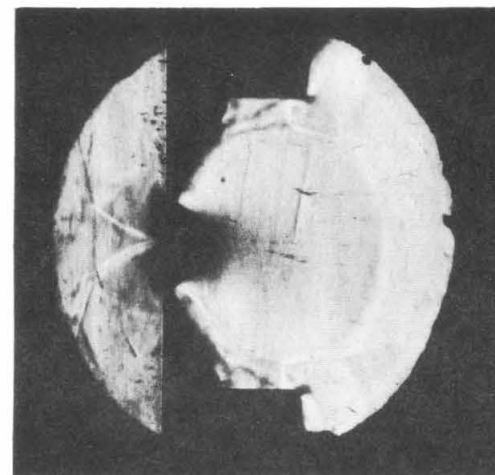
(a)

TIME DELAY = 20 MICROSECONDS



(b)

TIME DELAY = 30 MICROSECONDS



(c)

TIME DELAY = 40 MICROSECONDS

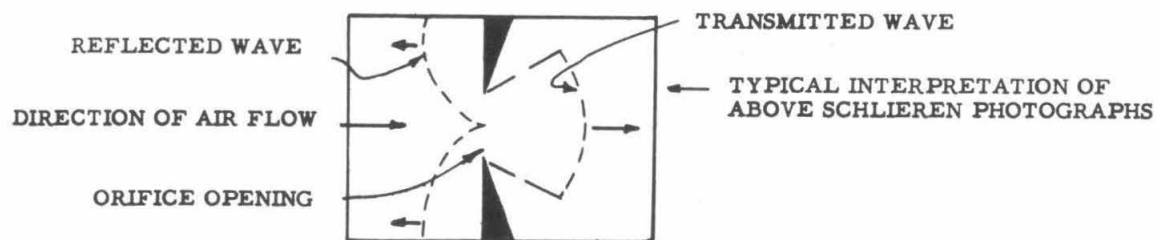
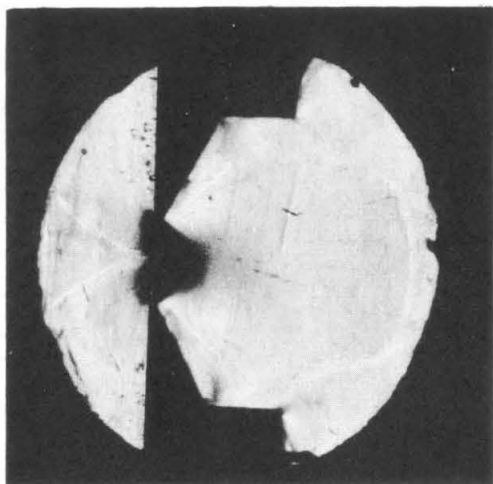
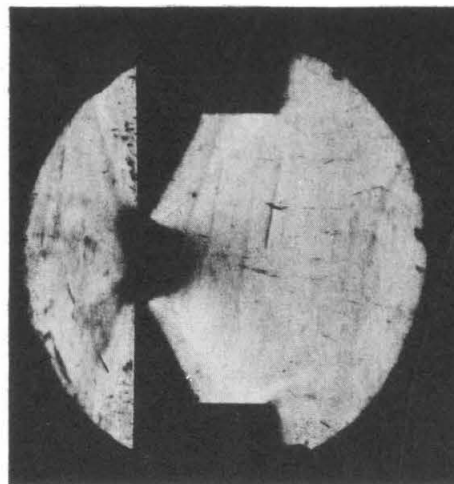


FIGURE 12

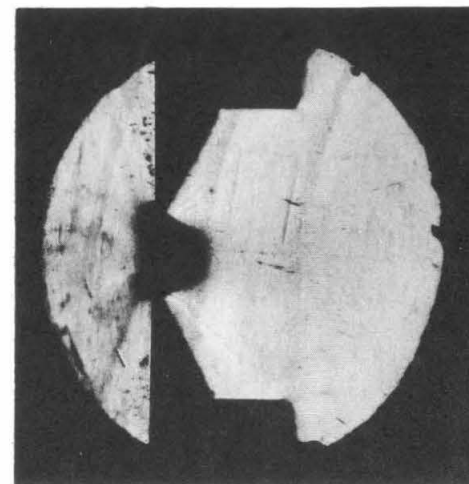
CONFIGURATION B, PLATE TYPE ORIFICE, SEQUENCE OF SCHLIEREN PHOTOGRAPHS SHOWING THE WAVES OF THE STARTING FLOW PROCESS AND THE TRANSMITTED WAVE, M_{sd}



(d)
TIME DELAY = 50 MICROSECONDS



(e)
TIME DELAY = 100 MICROSECONDS



(f)
TIME DELAY = 100 MICROSECONDS

FIGURE 12 (CONTINUED)
CONFIGURATION B, PLATE TYPE ORIFICE, SEQUENCE OF
SCHLIEREN PHOTOGRAPHS SHOWING THE WAVES OF THE
STARTING FLOW PROCESS AND THE TRANSMITTED WAVE, M_{sd}

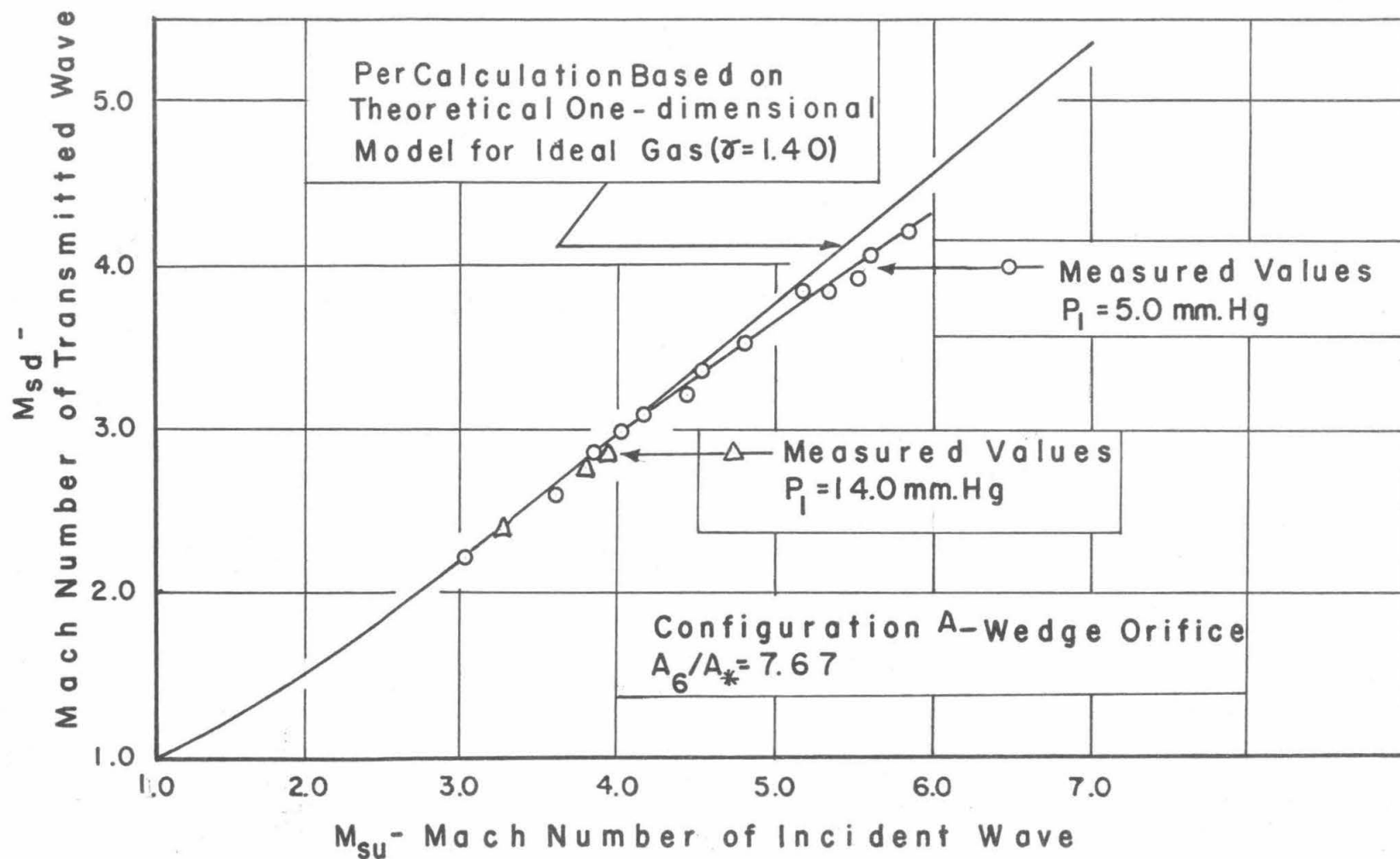


FIGURE 13

COMPARISON OF MEASURED VALUES AND THEORETICAL ONE DIMENSIONAL MODEL PREDICTED VALUES OF MACH NUMBER OF TRANSMITTED WAVE.
 CONFIGURATION A, WEDGE-TYPE ORIFICE, AREA RATIO $A_6/A_* = 7.67$

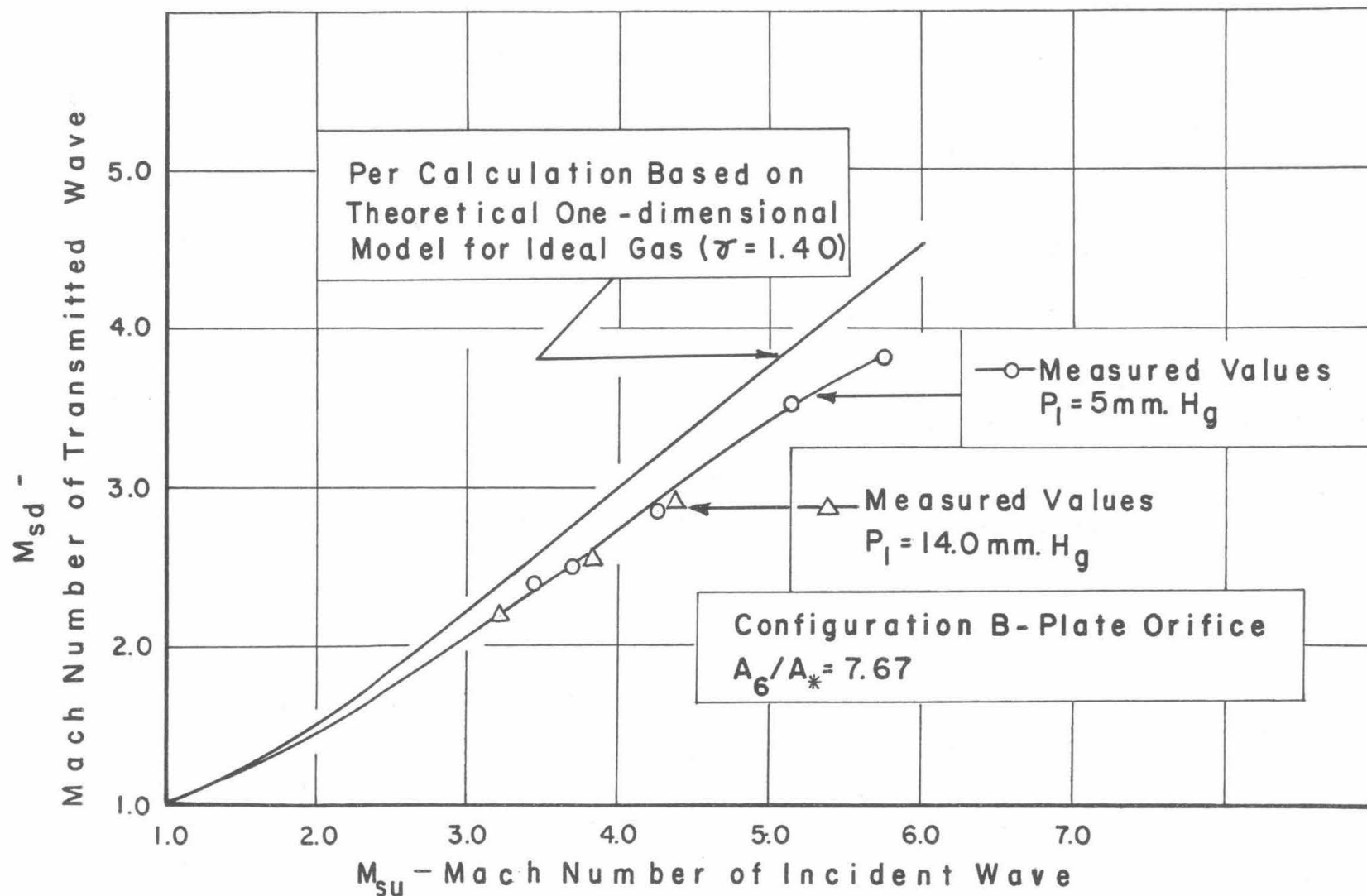


FIGURE 14

COMPARISON OF MEASURED VALUES AND THEORETICAL ONE DIMENSIONAL MODEL PREDICTED VALUES OF MACH NUMBER OF TRANSMITTED WAVE. CONFIGURATION B, PLATE-TYPE ORIFICE, AREA RATIO $A_6/A_* = 7.67$

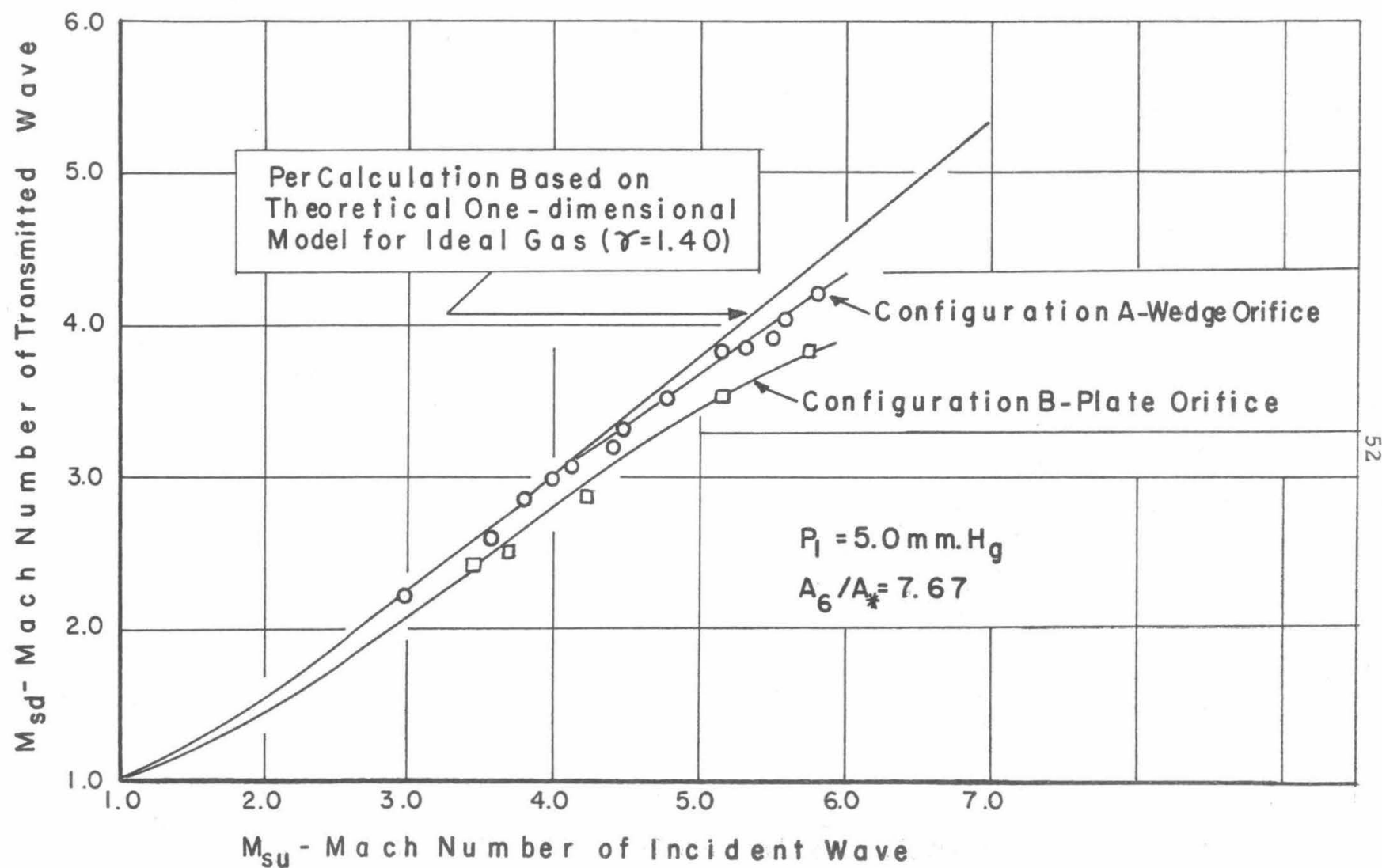


FIGURE 15
COMPARISON OF TRANSMITTED WAVE MACH NUMBERS OF CONFIGURATIONS A AND B

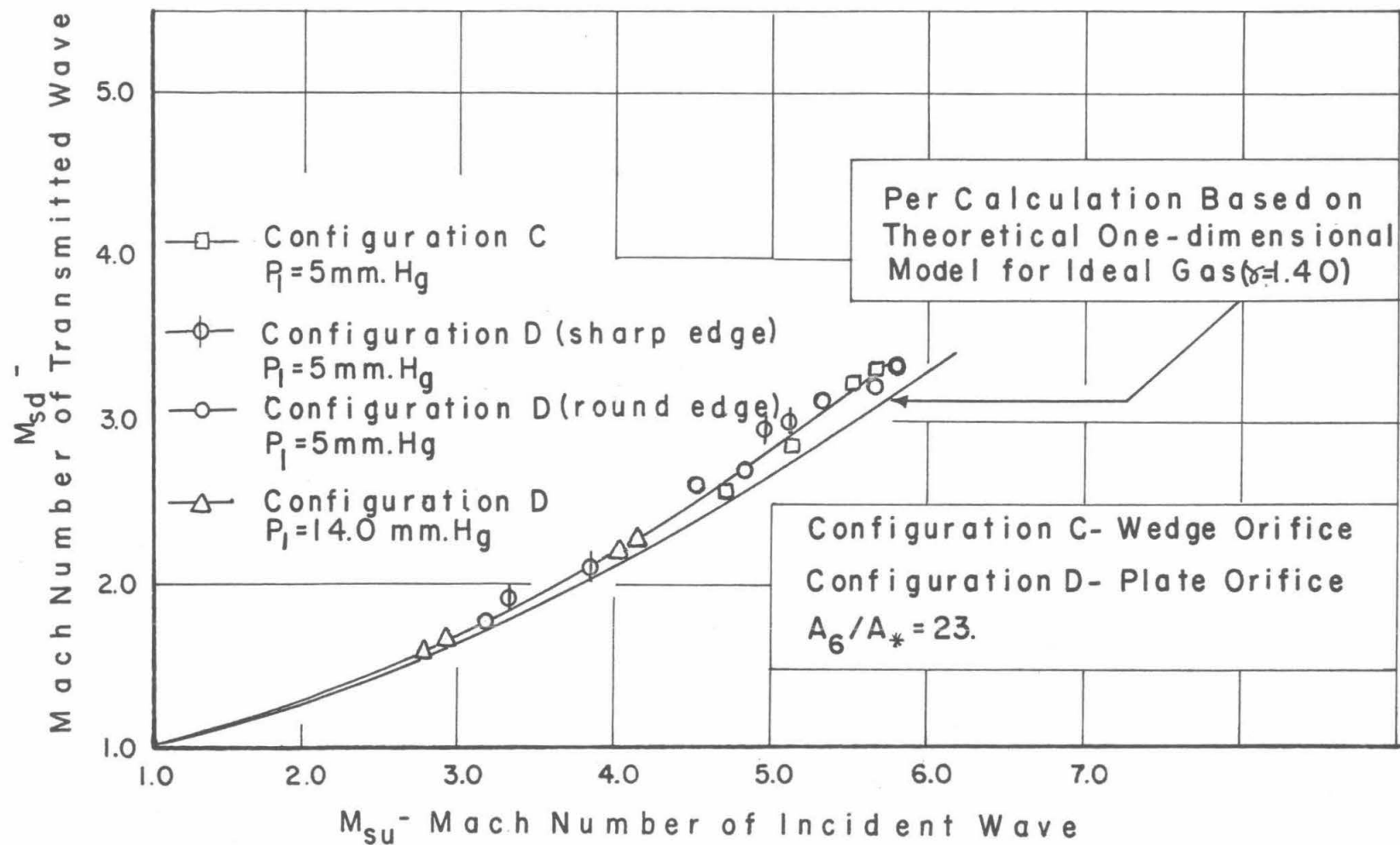


FIGURE 16

COMPARISON OF MEASURED VALUES AND THEORETICAL ONE DIMENSIONAL MODEL PREDICTED VALUES OF TRANSMITTED WAVE MACH NUMBERS. CONFIGURATIONS C AND D, AREA RATIO $A_6/A_* = 23$

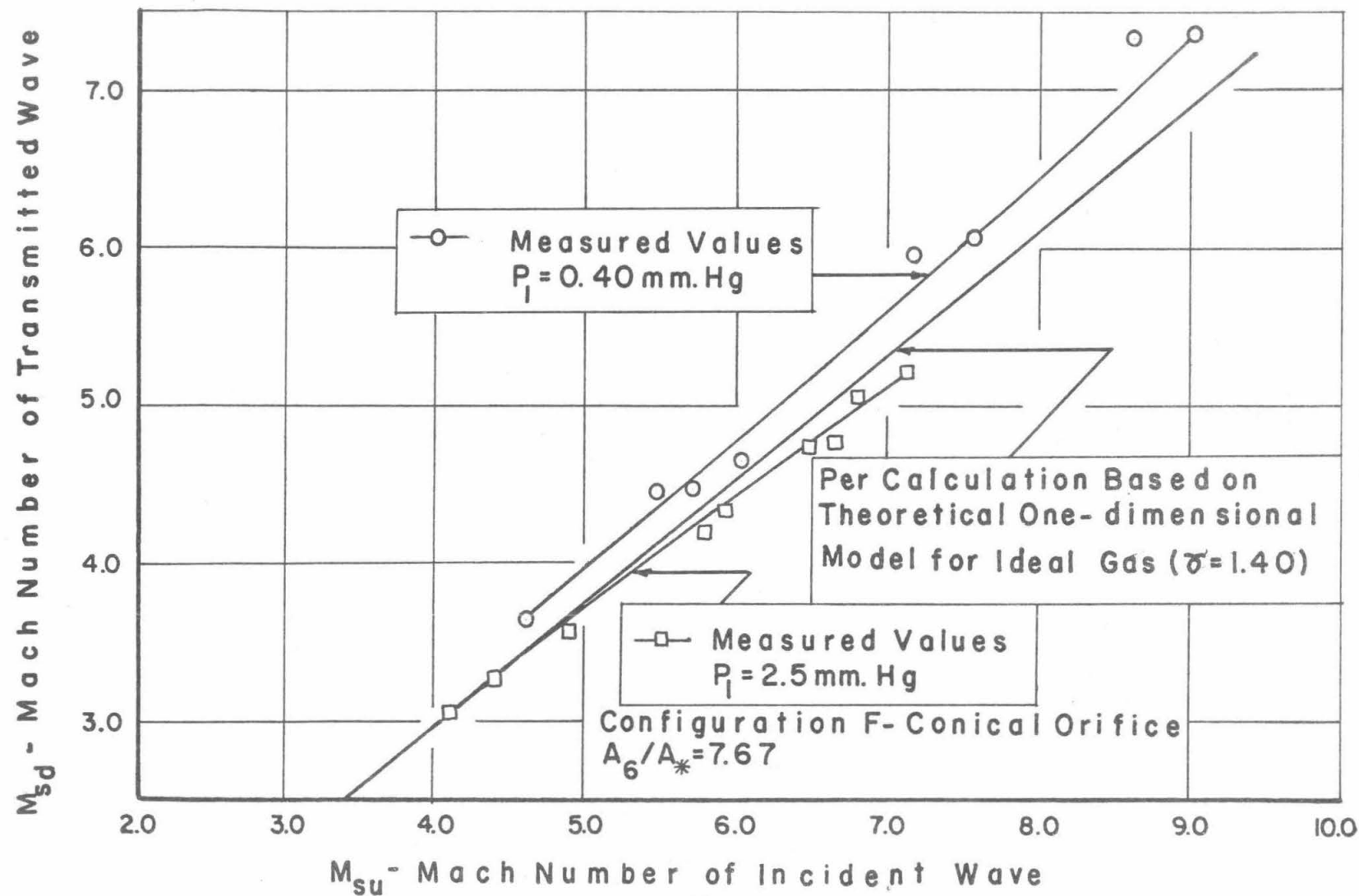


FIGURE 17

COMPARISON OF MEASURED VALUES AND THEORETICAL ONE DIMENSIONAL
MODEL PREDICTED VALUES OF TRANSMITTED WAVE MACH NUMBERS.
CONFIGURATION F, CONICAL TYPE ORIFICE, AREA RATIO $A_6/A_* = 7.67$

GUGGENHEIM AERONAUTICAL LABORATORY
CALIFORNIA INSTITUTE OF TECHNOLOGY

HYPERSONIC RESEARCH PROJECT
Contract No. DA-04-495-Ord-19

DISTRIBUTION LIST

U. S. Government Agencies

Los Angeles Ordnance District
55 South Grand Avenue
Pasadena 2, California
Attention: Mr. E. L. Stone
2 copies

Los Angeles Ordnance District
55 South Grand Avenue
Pasadena 2, California
Attention: ORDEV-00-
Mr. Z. Typaldos

Chief of Ordnance
Department of the Army
ORDTB - Ballistic Section
The Pentagon
Washington 25, D. C.
Attention: Mr. G. Stetson

Chief of Ordnance
Department of the Army
Washington 25, D. C.
Attention: ORDTB
For Transmittal To
Department of Commerce
Office of Technical Information

Chief of Ordnance
Department of the Army
Washington 25, D. C.
Attention: ORDGU-SE
For Transmittal To
Director of Intelligence
Headquarters, USAF
Washington 25, D. C.
Attention: Foreign Liaison Branch
For: The Aeronautical Research
Institute of Sweden
Ulvssunda 1, Sweden
Attention: Mr. Georg Drougge

Chief of Ordnance
Department of the Army
Washington 25, D. C.
Attention: ORDGU-SE
For Transmittal To
Canadian Joint Staff

Chief of Ordnance
Department of the Army
Washington 25, D. C.
Attention: ORDGU-SE
For Transmittal To
Foreign Relations Section
For Australian Joint Services Mission

Office of Ordnance Research
Box CM, Duke Station
Durham, North Carolina
10 copies

Ordnance Aerophysics Laboratory
Daingerfield, Texas
Attention: Mr. R. J. Valluz

Commanding Officer
Diamond Ordnance Fuze Laboratories
Washington 25, D. C.
Attention: ORDTL 06.33

Commanding General
Army Ballistics Missile Agency
Huntsville, Alabama
Attention: ORDAB-1P
2 copies

Commanding General
Army Ballistics Missile Agency
Huntsville, Alabama
Attention: ORDAB-DA
Mr. T. G. Reed
3 copies

Commanding General
Redstone Arsenal
Huntsville, Alabama
Attention: Technical Library

Commanding General
Redstone Arsenal
Huntsville, Alabama
Attention: Dr. E. Geissler

Chief of Staff
United States Army
The Pentagon
Washington 25, D. C.
Attention: Director/Research

Exterior Ballistic Laboratories
Aberdeen Proving Ground
Maryland
Attention: Mr. C. L. Poor

Ballistic Research Laboratories
Aberdeen Proving Ground
Maryland
Attention: Dr. Joseph Sternberg

Commanding General
White Sands Proving Ground
Las Cruces, New Mexico

Directorate of Advanced Studies
Air Force Office of Scientific Research
P. O. Box 2035-D
Pasadena 2, California
Attention: Dr. M. Alperin

Commander
Air Force
Office of Scientific Research
Washington 25, D. C.
Attention: RDTRRF

Mechanics Division
Air Force
Office of Scientific Research
Washington 25, D. C.

Air Force Armament Center
Air Research and Development
Command
Eglin Air Force Base
Florida
Attention: Technical Library

Air Research and Development
Command
European Office
Shell Building
60 Rue Rabenstein
Brussels, Belgium
Attention: Col. Lee Gossick, Chief
5 copies

Commander
Wright Air Development Center
Wright-Patterson Air Force Base
Ohio
Attention: WCLSR

Commander
Wright Air Development Center
Wright-Patterson Air Force Base
Ohio
Attention: WCLSW

Commander
Wright Air Development Center
Wright-Patterson Air Force Base
Ohio
Attention: WCLSW, Mr. P. Antonatos

Commander
Wright Air Development Center
Wright-Patterson Air Force Base
Ohio
Attention: Dr. H. K. Doetsch

Director of Research and Development
DCS/D
Headquarters
USAF
Washington 25, D. C.
Attention: AFDRD-RE

Commander
Western Development Division
P. O. Box 262
Ingelwood, California

Commander
Western Development Division
5760 Arbor Vitae Street
Los Angeles, California
Attention: Maj. Gen. B. A. Schriever

Commander
Arnold Engineering Development Center
Tullahoma, Tennessee
Attention: AEORL

Commander
 Arnold Engineering Development Center
 Tullahoma, Tennessee
 Attention: Col. F. H. Richardson

Air University Library
 Maxwell Air Force Base
 Alabama

Hollomann Air Force Base
 Alamogordo, New Mexico
 Attention: Dr. G. Eber

U. S. Naval Ordnance Laboratory
 White Oak
 Silver Spring, Maryland
 Attention: Dr. H. Kurzweg

U. S. Naval Ordnance Laboratory
 White Oak
 Silver Spring 19, Maryland
 Attention: Dr. R. K. Lobb

U. S. Naval Ordnance Laboratory
 White Oak
 Silver Spring 19, Maryland
 Attention: Dr. Z. I. Slawsky

U. S. Naval Ordnance Test Station
 China Lake
 Inyokern, California
 Attention: Mr. Howard R. Kelly, Head
 Aerodynamics Branch,
 Code 5032

Navy Department
 Bureau of Ordnance
 Technical Library
 Washington 25, D. C.
 Attention: Ad-3

Director
 Naval Research Laboratory
 Washington 25, D. C.

Office of Naval Research
 Department of the Navy
 Washington 25, D. C.

Commanding Officer
 Office of Naval Research
 Branch Office
 Navy, 100
 FPO
 New York, N. Y.
 2 copies

Commander
 U. S. Naval Proving Ground
 Dahlgren, Virginia

Bureau of Aeronautics
 Department of the Navy
 Room 2 w 75
 Washington 25, D. C.
 Attention: Mr. F. A. Loudon

Commander
 Armed Services Technical
 Information Agency
 Attention: TIPDR
 Arlington Hall Station
 Arlington 12, Virginia
 10 copies

National Bureau of Standards
 Department of Commerce
 Washington 25, D. C.
 Attention: Dr. G. B. Schubauer

National Advisory Committee
 for Aeronautics
 1512 H Street, N. W.
 Washington 25, D. C.
 Attention: Dr. H. L. Dryden, Director
 5 copies

National Advisory Committee
 for Aeronautics
 Ames Aeronautical Laboratory
 Moffett Field, California
 Attention: Mr. H. Julian Allen

National Advisory Committee
 for Aeronautics
 Ames Aeronautical Laboratory
 Moffett Field, California
 Attention: Dr. D. Chapman

National Advisory Committee
 for Aeronautics
 Ames Aeronautical Laboratory
 Moffett Field, California
 Attention: Dr. A. C. Charters

National Advisory Committee
for Aeronautics
Ames Aeronautical Laboratory
Moffett Field, California
Attention: Mr. A. J. Eggers

Technical Information Service
P. O. Box 62
Oak Ridge, Tennessee

National Advisory Committee
for Aeronautics
Ames Aeronautical Laboratory
Moffett Field, California
Attention: Dr. M. K. Rubesin

National Advisory Committee
for Aeronautics
Ames Aeronautical Laboratory
Moffett Field, California
Attention: Mr. J. R. Stalder

National Advisory Committee
for Aeronautics
Langley Aeronautical Laboratory
Langley Field, Virginia
Attention: Mr. M. Bertram

National Advisory Committee
for Aeronautics
Langley Aeronautical Laboratory
Langley Field, Virginia
Attention: Dr. A. Busemann

National Advisory Committee
for Aeronautics
Langley Aeronautical Laboratory
Langley Field, Virginia
Attention: Mr. C. McLellan

National Advisory Committee
for Aeronautics
Langley Aeronautical Laboratory
Langley Field, Virginia
Attention: Mr. John Stack

National Advisory Committee
for Aeronautics
Lewis Flight Propulsion Laboratory
Cleveland Municipal Airport
Cleveland 11, Ohio
Attention: Dr. J. C. Evvard

National Advisory Committee
for Aeronautics
Lewis Flight Propulsion Laboratory
Cleveland Municipal Airport
Cleveland 11, Ohio
Attention: Dr. A. Silverstein

Universities and Non-Profit Organizations

Brown University
Graduate Division of Applied Mathematics
Providence 12, Rhode Island
Attention: Professor W. Prager

Brown University
Graduate Division of Applied Mathematics
Providence 12, Rhode Island
Attention: Dr. R. Probst

University of California
Low Pressures Research
Institute of Engineering Research
Engineering Field Station
1301 South 46th Street
Richmond, California
Attention: Professor S. A. Schaaf

University of California at Los Angeles
Department of Engineering
Los Angeles 24, California
Attention: Dr. L. M. K. Boelter

Case Institute of Technology
Cleveland, Ohio
Attention: Dr. G. Kuerti

Catholic University of America
Department of Physics
Washington 17, D. C.
Attention: Professor K. F. Herzfeld

Cornell Aeronautical Laboratory
Buffalo, New York
Attention: Dr. A. Flax

Cornell University
Graduate School of Aeronautical Engineering
Ithaca, New York
Attention: Dr. W. R. Sears

Harvard University
Department of Applied Physics and
Engineering Science
Cambridge 38, Massachusetts
Attention: Dr. A. Bryson

Harvard University
Department of Applied Physics and
Engineering Science
Cambridge 38, Massachusetts
Attention: Dr. H. W. Emmons

University of Illinois
Department of Aeronautical Engineering
Urbana, Illinois
Attention: Professor C. H. Fletcher

The Johns Hopkins University
Applied Physics Laboratory
8621 Georgia Avenue
Silver Spring, Maryland
Attention: Dr. E. A. Bonney

The Johns Hopkins University
Applied Physics Laboratory
8621 Georgia Avenue
Silver Spring, Maryland
Attention: Dr. F. N. Frenkiel

The Johns Hopkins University
Applied Physics Laboratory
8621 Georgia Avenue
Silver Spring, Maryland
Attention: Dr. F. K. Hill

The Johns Hopkins University
Department of Aeronautical Engineering
Baltimore 18, Maryland
Attention: Dr. F. H. Clauser

The Johns Hopkins University
Department of Aeronautical Engineering
Baltimore 18, Maryland
Attention: Dr. L. Kovasznay

The Johns Hopkins University
Department of Mechanical Engineering
Baltimore 18, Maryland
Attention: Dr. S. Corrsin

Lehigh University
Physics Department
Bethlehem, Pennsylvania
Attention: Dr. R. Emrich

University of Maryland
Department of Aeronautical Engineering
College Park, Maryland
Attention: Dr. S. F. Shen

University of Maryland
Institute of Fluid Dynamics and
Applied Mathematics
College Park, Maryland
Attention: Director

University of Maryland
Institute of Fluid Dynamics and
Applied Mathematics
College Park, Maryland
Attention: Professor F. R. Hama

University of Maryland
Institute of Fluid Dynamics and
Applied Mathematics
College Park, Maryland
Attention: Dr. H. T. Yang

Massachusetts Institute of Technology
Cambridge 39, Massachusetts
Attention: Dr. A. H. Shapiro

Massachusetts Institute of Technology
Department of Aeronautical Engineering
Cambridge 39, Massachusetts
Attention: Professor M. Finston

Massachusetts Institute of Technology
Department of Aeronautical Engineering
Cambridge 39, Massachusetts
Attention: Dr. G. Stever

University of Michigan
Ann Arbor, Michigan
Attention: Dr. H. P. Liepmann

University of Michigan
Department of Aeronautical Engineering
East Engineering Building
Ann Arbor, Michigan
Attention: Dr. Arnold Kuethe

University of Michigan
Department of Aeronautical Engineering
East Engineering Building
Ann Arbor, Michigan
Attention: Professor W. C. Nelson

University of Michigan
Department of Aeronautical Engineering
Aircraft Propulsion Laboratory
Ann Arbor, Michigan
Attention: Mr. J. A. Nicholls

University of Michigan
Department of Physics
Ann Arbor, Michigan
Attention: Dr. O. Laporte

University of Minnesota
Department of Aeronautical Engineering
Minneapolis 14, Minnesota
Attention: Professor J. D. Akerman

University of Minnesota
Department of Aeronautical Engineering
Minneapolis 14, Minnesota
Attention: Dr. C. C. Chang

University of Minnesota
Department of Aeronautical Engineering
Minneapolis 14, Minnesota
Attention: Dr. R. Hermann

University of Minnesota
Department of Mechanical Engineering
Division of Thermodynamics
Minneapolis, Minnesota
Attention: Dr. E. R. G. Eckert

New York University
Department of Aeronautics
University Heights
New York 53, New York
Attention: Dr. J. F. Ludloff

New York University
Institute of Mathematics and Mechanics
45 Fourth Street
New York 53, New York
Attention: Dr. R. W. Courant

North Carolina State College
Department of Engineering
Raleigh, North Carolina
Attention: Professor R. M. Pinkerton

Ohio State University
Aeronautical Engineering Department
Columbus, Ohio
Attention: Professor A. Tifford

Ohio State University
Aeronautical Engineering Department
Columbus, Ohio
Attention: Professor G. L. von Eschen

University of Pennsylvania
Philadelphia, Pennsylvania
Attention: Professor M. Lessen

Polytechnic Institute of Brooklyn
Aerodynamic Laboratory
527 Atlantic Avenue
Freeport, New York
Attention: Dr. A. Ferri

Polytechnic Institute of Brooklyn
Aerodynamic Laboratory
527 Atlantic Avenue
Freeport, New York
Attention: Dr. P. Libby

Princeton University
Princeton, New Jersey
Attention: Dr. Sin I. Cheng

Princeton University
Forrestal Research Center
Princeton, New Jersey
Attention: Library

Princeton University
Aeronautics Department
Forrestal Research Center
Princeton, New Jersey
Attention: Professor S. Bogdonoff

Princeton University
Aeronautics Department
Forrestal Research Center
Princeton, New Jersey
Attention: Dr. L. Crocco

Princeton University
Aeronautics Department
Forrestal Research Center
Princeton, New Jersey
Attention: Professor Wallace Hayes

Princeton University
Palmer Physical Laboratory
Princeton, New Jersey
Attention: Dr. W. Bleakney

Purdue University
School of Aeronautical Engineering
Lafayette, Indiana
Attention: Librarian

Rensselaer Polytechnic Institute
Aeronautics Department
Troy, New York
Attention: Dr. R. P. Harrington

Rensselaer Polytechnic Institute
Aeronautics Department
Troy, New York
Attention: Dr. T. Y. Li

Rouss Physical Laboratory
University of Virginia
Charlottesville, Virginia
Attention: Dr. J. W. Beams

University of Southern California
Aeronautical Laboratories Department
Box 1001
Oxnard, California
Attention: Mr. J. H. Carrington,
Chief Engineer

Stanford University
Department of Mechanical Engineering
Palo Alto, California
Attention: Dr. D. Bershader

University of Texas
Defense Research Laboratory
500 East 24th Street
Austin, Texas
Attention: Professor M. J. Thompson

University of Washington
Department of Aeronautical Engineering
Seattle 5, Washington
Attention: Professor F. S. Eastman

University of Washington
Department of Aeronautical Engineering
Seattle 5, Washington
Attention: Professor R. E. Street

University of Wisconsin
Department of Chemistry
Madison, Wisconsin
Attention: Dr. J. O. Hirschfelder

Institute of the Aeronautical Sciences
2 East 64th Street
New York 21, New York
Attention: Library

Midwest Research Institute
4049 Pennsylvania
Kansas City, Missouri
Attention: Mr. M. Goland, Director
for Engineering Sciences

National Science Foundation
Washington 25, D. C.
Attention: Dr. J. McMillan

National Science Foundation
Washington 25, D. C.
Attention: Dr. R. Seeger

Industrial Companies

Aeronutronic Systems, Inc.
1234 Air Way
Glendale, California
Attention: Dr. J. Charyk

Aeronutronic Systems, Inc.
1234 Air Way
Glendale, California
Attention: Dr. L. Kavanau

Aerophysics Development Corp.
P. O. Box 689
Santa Barbara, California
Attention: Librarian

ARO, Inc.
P. O. Box 162
Tulahoma, Tennessee
Attention: Dr. B. Goethert

ARO, Inc.
P. O. Box 162
Tulahoma, Tennessee
Attention: Librarian,
Gas Dynamics Facility

AVCO Manufacturing Corp.
2385 Revere Beach Parkway
Everett 49, Massachusetts
Attention: Library

AVCO Manufacturing Corp.
2385 Revere Beach Parkway
Everett 49, Massachusetts
Attention: Dr. A. Kantrowitz

Bell Aircraft Corp.
Aerodynamics Section
P. O. Box 1
Buffalo 5, New York
Attention: Dr. Joel S. Isenberg

Boeing Airplane Company
P. O. Box 3107
Seattle 14, Washington
Attention: Mr. G. Snyder

Chance Vought Aircraft, Inc.
P. O. Box 5907
Dallas, Texas
Attention: Mr. J. R. Clark

Chance Vought Aircraft, Inc.
P. O. Box 5907
Dallas, Texas
Attention: Dr. R. Wilson

CONVAIR
A Division of General Dynamics Corp.
San Diego 12, California
Attention: Mr. C. Bossart

CONVAIR
A Division of General Dynamics Corp.
San Diego 12, California
Attention: Mr. W. H. Dorrance
Dept. 1-16

CONVAIR
A Division of General Dynamics Corp.
San Diego 12, California
Attention: Mr. W. B. Mitchell

CONVAIR
A Division of General Dynamics Corp.
Fort Worth 1, Texas
Attention: Mr. W. B. Fallis

CONVAIR
A Division of General Dynamics Corp.
Fort Worth 1, Texas
Attention: Mr. E. B. Maske

CONVAIR
A Division of General Dynamics Corp.
Fort Worth 1, Texas
Attention: Mr. W. G. McMullen

CONVAIR
A Division of General Dynamics Corp.
Fort Worth 1, Texas
Attention: Mr. R. H. Widmer

Cooperative Wind Tunnel
950 South Raymond Avenue
Pasadena, California
Attention: Mr. F. Felberg

Cooperative Wind Tunnel
950 South Raymond Avenue
Pasadena, California
Attention: Mr. E. I. Pritchard

Douglas Aircraft Company
Santa Monica, California
Attention: Mr. J. Gunkel

Douglas Aircraft Company
Santa Monica, California
Attention: Mr. Ellis Lapin

Douglas Aircraft Company
Santa Monica, California
Attention: Mr. H. Luskin

Douglas Aircraft Company
Santa Monica, California
Attention: Dr. W. B. Oswald

General Electric Company
Research Laboratory
Schenectady, New York
Attention: Dr. H. T. Nagamatsu

General Electric Company
Missile and Ordnance Systems Dept.
3198 Chestnut Street
Philadelphia 4, Pennsylvania
Attention: Documents Library,
L. Chasen, Mgr. - Libraries

The Glenn L. Martin Company
Aerophysics Research Staff
Flight Vehicle Division
Baltimore 3, Maryland
Attention: Dr. Mark V. Morkovin

The Glenn L. Martin Company
Baltimore 3, Maryland
Attention: Mr. G. S. Trimble, Jr.

Grumman Aircraft Engineering Corp.
Bethpage, New York
Attention: Mr. C. Tilgner, Jr.

Hughes Aircraft Company
Culver City, California
Attention: Dr. A. E. Puckett

Lockheed Aircraft Corp.
Missiles Division
Van Nuys, California
Attention: Library

Lockheed Missiles Systems Division
Research and Development Laboratory
Sunnyvale, California
Attention: Dr. W. Griffith

Lockheed Missiles Systems Division
P. O. Box 504
Sunnyvale, California
Attention: Dr. L. H. Wilson

Lockheed Missiles Systems Division
Lockheed Aircraft Corp.
Palo Alto, California
Attention: Mr. R. Smelt

Lockheed Missiles Systems Division
Lockheed Aircraft Corp.
Palo Alto, California
Attention: Mr. Maurice Tucker

Marquardt Aircraft Company
P. O. Box 2013 - South Annex
Van Nuys, California
Attention: Mr. E. T. Pitkin

McDonnell Aircraft Corp.
Lambert-St. Louis Municipal Airport
P. O. Box 516
St. Louis 3, Missouri
Attention: Mr. K. Perkins

North American Aviation, Inc.
Aeronautical Laboratory
Downey, California
Attention: Dr. E. R. Van Driest

Northrop Aircraft, Inc.
1001 East Broadway
Hawthorne, California
Attention: Mr. E. Schmued

Ramo-Wooldridge Corporation
409 East Manchester Blvd.
Inglewood, California
Attention: Dr. M. U. Clauser

Ramo-Wooldridge Corporation
409 East Manchester Blvd.
Inglewood, California
Attention: Dr. Louis G. Dunn

The RAND Corporation
1700 Main Street
Santa Monica, California
Attention: Librarian

The RAND Corporation
1700 Main Street
Santa Monica, California
Attention: Dr. C. Gazley

The RAND Corporation
1700 Main Street
Santa Monica, California
Attention: Mr. E. P. Williams

Republic Aviation Corporation
Conklin Street
Farmingdale, L. I., New York
Attention: Dr. W. J. O'Donnell

United Aircraft Corporation
East Hartford, Connecticut
Attention: Mr. J. G. Lee

Internal

Dr. Harry Ashkenas
Dr. Frank E. Goddard
Dr. James M. Kendall
Dr. John Laufer
Dr. Thomas Vrebalovich
Dr. Peter P. Wegener
Hypersonic WT; Attn: Mr. G. Goranson
Reports Group
Jet Propulsion Laboratory
4800 Oak Grove Drive
Pasadena 2, California

Dr. W. D. Rannie
Goddard Professor
Jet Propulsion Center
California Institute of Technology

Dr. Julian D. Cole
Dr. Donald E. Coles
Dr. P. A. Lagerstrom
Prof. Lester Lees
Dr. H. W. Liepmann
Dr. Clark B. Millikan
Dr. Anatol Roshko

Aeronautics Library
Hypersonic Staff and Research Workers (20)
Hypersonic Files (3)

Foreign

via AGARD Distribution Centers